

Department of Physics and Astronomy  
University of Heidelberg

Master Thesis in Physics  
submitted by

**Daniel Wiegand**

born in Heppenheim (Germany)

**2013**



# MadMax

This Master Thesis has been carried out by Daniel Wiegand at the  
Institute for Theoretical Physics (ITP) in Heidelberg  
under the supervision of  
Prof. Tilman Plehn



## Abstract

The discovery of a Higgs boson at LHC is only a first step of taking our knowledge of fundamental interactions to the test. To find out more about the nature of electroweak symmetry breaking in the Standard Model, it is crucial to measure all properties of the Higgs. It is crucial to optimize the signal over background ratio in order to get the best measurement. For this we need to identify the corresponding phase space. As it turns out the best discriminating variable for doing so is the so-called Log-Likelihood.

We present the tool **MadMax**, which was built from the parton level event generator **MadEvent**, to perform the core calculations for the Log-Likelihood. It is specifically designed with LHC Higgs searches in mind but in principle is applicable to any process that **MadGraph** can produce. The approach taken is based on the Neyman-Pearson lemma for hypothesis tests.

The tool represents a automatization of concepts originally presented in [1]. As applications we present the maximum expected significances for (i) a Higgs produced in Weak Boson Fusion decaying to a  $\mu^+\mu^-$  pair and (ii) one produced in Higgs-Strahlung decaying to a  $b\bar{b}$  pair.

## Zusammenfassung

Die Entdeckung eines Higgs Bosons am LHC ist nur ein erster Schritt um unser Verständnis fundamentaler Wechselwirkungen zu überprüfen. Um den elektroschwachen Symmetriebruch im Standardmodell zu verstehen müssen alle Eigenschaften des Higgs vermessen werden. Hierfür muss das Verhältnis von Signal über Untergrund optimiert werden. Wie sich herausstellt ist der beste Weg dies zu tun mittels eines Log-Likelihoods.

Wir stellen das tool **MadMax** vor, das auf dem Parton-level Event generator **MadEvent** basiert und die grundlegenden Berechnungen des Log-Likelihoods ausführt. Es wurde speziell für die Higgssuche am LHC entwickelt ist aber im Prinzip für jeden Prozess den **MadGraph** beherrscht einsetzbar. Unsere Herangehensweise basiert auf dem Neyman-Pearson lemma für Hypothesentests.

Das tool ist eine Automatisierung des Vorgehens, das ursprünglich in [1] vorgestellt wurde. Als Anwendung präsentieren wir eine Analyse (i) der Higgsproduktion mittels Weak Boson Fusion und anschließendem Zerfall zu einem  $\mu^+\mu^-$  Paar und (ii) Higgsproduktion durch Higgs-Strahlung mit Zerfall nach einem  $b\bar{b}$  Paar.



# Contents

<b>1</b>	<b>Introduction</b>	<b>1</b>
<b>2</b>	<b>Theoretical Concepts</b>	<b>3</b>
2.1	The Standard Model . . . . .	3
2.1.1	Electroweak Symmetry-Breaking . . . . .	4
2.1.2	QCD . . . . .	8
2.2	Monte Carlo Integration and Event Generation . . . . .	8
2.2.1	Cross Sections and Phase Space Integrals . . . . .	8
2.2.2	Monte-Carlo Techniques . . . . .	9
2.2.3	The Single Diagram Enhanced Method . . . . .	11
2.3	The Log-Likelihood Analysis . . . . .	12
2.3.1	Exclusion Limits . . . . .	12
2.3.2	The Maximum Likelihood Method . . . . .	13
2.3.3	On the Way to MadMax . . . . .	16
<b>3</b>	<b>From MadGraph to MadMax</b>	<b>18</b>
3.1	The Integration routines in MadGraph5 . . . . .	18
3.2	Construction and Implementation . . . . .	21
3.3	Control of the MadMax Results . . . . .	24
3.4	Higgs-production in WBF and successive decay to a $\mu^+\mu^-$ pair . . . . .	25
3.4.1	The Process . . . . .	25
3.4.2	Detector Effects . . . . .	26
3.4.3	Results of the Analysis . . . . .	27
<b>4</b>	<b>Higgs-Strahlung and decay to <math>b\bar{b}</math> - Beyond Thunderdome</b>	<b>30</b>
4.1	Setting up the Process . . . . .	30
4.2	Results of the Analysis . . . . .	31
<b>5</b>	<b>Conclusions and Outlook</b>	<b>35</b>
<b>A</b>	<b>Set-Up of the WBF Processes in MadGraph5</b>	<b>39</b>
A.1	Signal-Process . . . . .	39
A.1.1	Correcting the Higgs Width . . . . .	39
A.1.2	The CKM Matrix . . . . .	40
A.1.3	Implementable Cuts . . . . .	40
A.2	Background-Processes . . . . .	41
A.2.1	Electroweak Background . . . . .	41
A.2.2	QCD Background . . . . .	43
<b>B</b>	<b>Comparison of the MadGraph5 and the MadMax-Integration</b>	<b>44</b>
B.1	Purely Leptonic Processes . . . . .	44

<u>Contents</u>	5
B.2 Semi-Leptonic Processes . . . . .	45
B.3 Purely Hadronic Processes . . . . .	46
<b>Bibliography</b>	<b>50</b>



# Chapter 1

## Introduction

The discovery of the scalar resonance with a mass of 126GeV by the ATLAS [2] and the CMS [3] experiments at LHC is maybe the greatest scientific discovery of the last decade.

A lot of indicators suggest that it indeed is the elusive Higgs boson predicted by the Standard Model of particle physics (SM). This particle is a remnant of the mechanism of electroweak symmetry breaking (EWSB). The mass of the resonance found lies within the range of masses allowed for the Higgs by theoretical constraints (unitarity bound, etc.) and its scalar nature has been confirmed. Those observations are however insufficient to make the claim that it is exactly the Higgs predicted. We have to exclude the possibility that a scalar particle from an alternative theory was found. Therefore, all properties associated with the SM-Higgs must be examined. These include the Yukawa couplings to the matter particles as well as the gauge couplings to the gauge bosons. Furthermore, one has to look at the cubic and quartic Higgs self-couplings deriving from the form of the Higgs potential.

In some sense the discovery of this particle is not "the last piece of the puzzle" but the first step in understanding the nature of symmetry breaking at the electroweak scale. Only through that way we can learn about the origin of mass generation just as well as understand how this seemingly arbitrary scale comes about and how it stabilizes. This is the main concern at LHC and its planned successors like ILC.

The urgent question to be asked before one can even begin to start looking for clues and answers is to find out where to start, to be more precise: Where do I have to look so my chances of getting a conclusive answer are best?

This question factorizes into two parts: (i) which production and decay channels are most suitable to deliver the information most telling of the Higgs properties? (ii) In which scenarios are they available in the first place? The answers to those are theoretically well established for the Standard Model. A good overview over the main channels and scenarios for LHC Higgs searches is given in [4].

In this thesis, we will be dealing with the task to determine under which circumstances most information can be extracted? Circumstances referring here to which parts of phase space are actually contributing most to the accumulation of signal. So we are looking for the regions in which the signature of the signal process is least contaminated by background.

Since a detector is, in general, only able to detect the final states of a certain process, we always have to fight to distinguish the signal i.e. the processes we are actually interested in from backgrounds imitating our signal. Nobody knows ad hoc if an excess in the data is actually caused by, say, a Higgs decaying or just random background processes producing a mimicking amount of decay products. To tell them apart we heavily rely on distinct features in the distributions of certain kinematic variables. The more distinct the distribution the less likely it is to be a random excess. One introduces the notion of significance to measure how distinct the signal signature differs from the background-only one. The significance of an observed signal over the background can be elegantly formalized through the so-called Log-Likelihood method. This method tells us

how likely (hence the name) it is for a set of background processes to fluctuate in a way that it could reproduce an observed signal. This makes a quantitative statement about the likeliness of our initial hypothesis.

The main scope of this thesis is to present a new tool **MadMax** which is based on the event generator **MadEvent**. It is part of the multi-purpose generator **MadGraph5** [5], [6]. This generator is an efficient way to handle the vast amount of processes happening in real experiments. Our tool enables one to calculate the significance of a given signal over irreducible backgrounds, over the entire or part of the phase space. It relies on the amplitudes generated by **MadGraph5** but performs most of its integrations stand-alone. We are then put in the position to iteratively decrease the size of the phase space, which we integrate out, and thus find the regions that contribute most to the increase of significance. These regions are the ones a search should focus on. Since **MadGraph5** was developed for essentially any kind of model tested at any kind of collider, **MadMax** is also not limited to LHC Higgs searches but can, in general, be used for any new physics exploration.

We start by reviewing the theoretical concepts paramount to the construction of **MadMax**. These include the physics of the Standard Models and electroweak symmetry breaking (since this was the goal we had initially in mind), Monte Carlo Methods and Event generators, and the mathematics behind the Likelihood method. After that, we describe the conceptual ideas behind **MadMax** and outline how it fundamentally differs from **MadGraph5**, in which it has since been integrated. In the last chapter we demonstrate its use and potential, by reproducing the analysis originally performed by [7]. Lastly we apply it to another Higgs production channel and examine Higgs-Strahlung with the Higgs decaying to  $b\bar{b}$  pairs afterwards.

The work presented in this thesis was done together with Tilman Plehn and Peter Schichtel at the Institute for Theoretical Physics, Heidelberg, and is largely based on ideas and concepts originally found in [1].

# Chapter 2

## Theoretical Concepts

### 2.1 The Standard Model

Our best description of interactions between particles on a quantum level is the Standard Model of Particle Physics (SM). It rests on a couple of very general a-priori assumptions that seem in the end to be justified by the model's high predictive power and accuracy. A detailed description of quantum field theory in general, and the Standard Model in particular, can be found in [8] and with a focus on LHC-phenomenology in [9]. Throughout this thesis we make use of Srednickis conventions and notations.

The SM matter particles are fermions which are arranged in three generations, each consisting of an electrically charged lepton, a neutral neutrino, an up- and a down-type quark.

Gen.	quarks	masses	charge	leptons	masses	charge
I	up	$2.3^{+0.7}_{-0.5}$ MeV	$+2/3$	electron $e^-$	511keV	-1
	down	$4.8^{+0.7}_{-0.3}$ MeV	$-1/3$	$e^-$ neutrino	$< 2.3\text{eV}$	0
II	charm	$1.3 \pm 0.03$ GeV	$+2/3$	muon $\mu^-$	105.7 MeV	-1
	strange	$95 \pm 5$ MeV	$-1/3$	$\mu^-$ neutrino	$< 0.2\text{MeV}$	0
III	top	$173.1 \pm 1.4$ GeV	$+2/3$	tau-lepton $\tau^-$	1.8GeV	-1
	bottom	$4.2 \pm 0.03$ GeV	$-1/3$	$\tau^-$ neutrino	$< 18.2\text{MeV}$	0

TABLE 2.1: The Standard Model fermions (mass values taken from the PDG [10])

We start the construction of the SM-Lagrangian by assuming that all these fermions are described by Dirac spinors whose dynamics are governed by the Dirac Lagrangian

$$\mathcal{L} = \bar{\Psi} (i\gamma_\mu \partial^\mu - m_\Psi) \Psi. \quad (2.1)$$

To make this free theory interacting we couple these fields to bosonic gauge fields - the force-carriers - in a canonical way by imposing an internal gauge symmetry. First note that the Lagrangian enjoys and can be done invariance under special unitary transformations  $SU(N)$ . These transformations take the explicit form

$$\Psi \rightarrow U(\alpha)\Psi \quad \text{and} \quad \bar{\Psi} \rightarrow \bar{\Psi}U^\dagger(\alpha) \quad \text{with} \quad U(\alpha) = \exp(i g \alpha^i T_i). \quad (2.2)$$

Here  $\alpha_i T^i$  is a linear combination of the  $N^2 - 1$  generator matrices  $T_i$  of the underlying  $su(N)$  algebra. Note that this transformation only makes sense if the spinors are arranged in  $SU(N)$   $N$ -tuples, which we implicitly assumed is the case. These are global symmetries of the Lagrangian which give rise to conserved Noether currents.

The underlying principle for introducing interactions is to assume that the coefficients  $\alpha_i$  are

local. Locality here is meant in the sense that their values become space-time dependent. This evidently spoils our invariance because the Lagrangian picks up terms from the derivative acting on  $\alpha_i(x)$  when transforming the fields in the Lagrangian. The way to deal with this is to add new fields (the gauge fields  $A_\mu^i$ ) that transform under the gauge transformation in such a manner as to cancel all of the invariance-violating terms. This is achieved by transforming all partial derivatives in the Dirac Lagrangian to so-called gauge covariant ones:

$$D_\mu = \partial_\mu - igA_\mu \quad \text{with} \quad A_\mu = A_\mu^i T_i. \quad (2.3)$$

This makes the Lagrangian invariant again, if and only if, the new fields transform under  $SU(N)$  as  $A_\mu \rightarrow U(\alpha)A_\mu U^\dagger(\alpha) + \frac{i}{g}U(\alpha)\partial_\mu U^\dagger(\alpha)$ .

We see now that the Lagrangian describes not only the dynamics of the fermion fields but also their coupling to gauge fields. The only thing apparently missing is the dynamics of the gauge fields themselves. Guided by the form of the electromagnetic Faraday tensor  $F_{\mu\nu}$  we define a generalized field strength tensor to introduce derivative terms of the gauge fields

$$F_{\mu\nu} = \frac{i}{g} [D_\mu, D_\nu] \quad \text{with} \quad F_{\mu\nu} \rightarrow U(\alpha)F_{\mu\nu}U^\dagger(\alpha). \quad (2.4)$$

A quadratic term in the field strength is a both Lorentz scalar and has correct mass dimension but would only almost transform correctly under  $SU(N)$ ; it would spoil the newly-constructed gauge invariance. If we exploit on the other hand the cyclic properties of the trace, we can write down a gauge field Lagrangian that is indeed  $SU(N)$  invariant.

$$\mathcal{L}_{\text{gauge}} = -\frac{1}{2}\text{Tr}(F^{\mu\nu}F_{\mu\nu}). \quad (2.5)$$

The prefactors are purely conventional. The only other term we can write down that respects all the symmetries and renormalizability includes the dual field strength tensor  $\tilde{F}^{\mu\nu} = \epsilon^{\mu\nu\rho\sigma}F_{\rho\sigma}$ .  $\tilde{F}^{\mu\nu}F_{\mu\nu}$  is however CP-odd which is not well-observed experimentally.

The full Lagrangian describes now a theory that contains the dynamics of all matter and force fields plus the interactions between them. The only thing left to do is to chose the gauge group in a smart way so the model matches observation.

### 2.1.1 Electroweak Symmetry-Breaking

The full gauge group of the Standard Model turns out to be  $SU(3)_c \times SU(2)_L \times U(1)_Y$ . The Labels  $c$  and  $Y$  represent the Noether charges under the symmetry group -  $Y$  we call the hypercharge while the charge for  $SU(2)$  is the weak isospin  $I$  and  $c$  refers to the color charge. The index  $L$  refers to the chiral nature of  $SU(2)$ . A theory built from this group in the way outlined actually enables us to describe all known interactions in nature sans gravity.

Two of the interactions we wish to describe are the weak force mediated through  $Z$  and  $W^\pm$  bosons and electromagnetism which is mediated by photons. To this end Glashow first proposed and worked out a gauge theory based on  $SU(2)_L \times U(1)_Y$ . Salam and Weinberg later extended it to account for the masses of the weak gauge bosons. The generators  $T_i$  for  $SU(2)$  are essentially rescaled Pauli matrices  $T_i = \frac{1}{2}\sigma_i$  obeying  $[T_i, T_j] = \epsilon_{ijk}T^k$  while for  $U(1)$  it is a multiplication of the field operator with an unimodular number.

From experiment we know that only left-handed particles couple to the weak bosons - or in other words: only the left-handed ones take part in the interactions. To satisfy observation this means that the fields charged under  $SU(2)_L$  must necessarily only they transform as doublets. The chiral fields are defined via the projection operators  $P_{L/R}$ :

$$\Psi_{L/R} = P_{L/R}\Psi = \frac{1}{2}(1 \mp \gamma_5)\Psi. \quad (2.6)$$

Additionally, it seems that the neutrinos are the only fermion fields that do not exist with a right-handed chirality.

To formulate the electroweak chiral Lagrangian we chose the left-handed doublets to be

$$\begin{pmatrix} \nu^m \\ l^m \end{pmatrix} = \begin{pmatrix} \nu_e \\ e^- \end{pmatrix}_L, \begin{pmatrix} \nu_\mu \\ \mu^- \end{pmatrix}_L, \begin{pmatrix} \nu_\tau \\ \tau^- \end{pmatrix}_L \quad \text{and} \quad \begin{pmatrix} U^m \\ D^m \end{pmatrix} = \begin{pmatrix} u \\ d \end{pmatrix}_L, \begin{pmatrix} s \\ c \end{pmatrix}_L, \begin{pmatrix} b \\ t \end{pmatrix}_L, \quad (2.7)$$

for quarks and leptons respectively. The index  $m$  labels the generation. The right-handed fields transform as the corresponding singlets under  $SU(2)$ .

Now we could go ahead and construct said electroweak Lagrangian as described in the first section. To write down the covariant derivatives that couple the fermions to the gauge fields, we need to stipulate under which representations the matter fields should transform, i.e. the internal quantum numbers.

Table 2.2 summarizes all the necessary information for the full gauge group before and after electroweak symmetry breaking.

	$SU(3)_c \times SU(2)_L \times U(1)_Y$		$SU(3)_c \times U(1)_{em}$
RH up-type	$(3, 1, -\frac{2}{3})$	RH up-type	$(3, -\frac{2}{3})$
RH down-type	$(3, 1, +\frac{1}{3})$	RH down-type	$(3, +\frac{1}{3})$
RH lepton	$(1, 1, +1)$	RH lepton	$(1, +1)$
Doublet $L_L$	$(1, 2, -\frac{1}{2})$	LH lepton	$(1, -1)$
		LH neutrino	$(1, 0)$
Doublet $Q_L$	$(3, 2, \frac{1}{6})$	LH up-type	$(3, \frac{2}{3})$
		LH down-type	$(3, -\frac{1}{3})$

TABLE 2.2: The representations under which the matter fields transform for the SM gauge group before symmetry breaking (left) and after (right). The actual quantum numbers are adapted from [8].

Notice that the Noether charge  $Q$  of the unbroken  $U(1)_{em}$  is linked to the ones of the broken  $SU(2)_L \times U(1)_Y$  via the Gell-Mann Nishijima relation

$$Q = I_3 + Y. \quad (2.8)$$

$I_3$  is the third component of the weak isospin which comes from the third generator  $T_3$  of  $SU(2)$  while  $Q$  turns out to be the physical electric charge.

If we proceed in setting up our model we stumble across a problem. From experiment we know that the weak gauge-bosons are anything but massless. Were we to write down a naïve mass term for them we would spoil gauge invariance. Even worse is that we cannot write down mass terms for the fermion fields either; this is due to the fact that  $SU(2)$  treats fields differently based on their chirality. Hence terms quadratic in the field operators are mixing left- and right-handed fields which immediately spoils gauge invariance as well.

This apparent problem can be fixed very elegantly by introducing four new scalar degrees of freedom, the Higgs field  $\Phi$  into the model. We assume the new field transforms in the  $(1, 2, -\frac{1}{2})$  representation of the full group.

$$\Phi = \begin{pmatrix} \phi^0 \\ \phi^- \end{pmatrix}, \quad (2.9)$$

where  $\phi^0$  and  $\phi^-$  are complex scalar fields.

The original mechanism was established by various people simultaneously and can be found e.g. in [11] and [12].

The Lagrangian governing the dynamics of this scalar doublet and the interactions of it with the gauge fields then looks like

$$\mathcal{L}_{\text{Higgs}} = \frac{1}{2} (D_\mu \Phi)^\dagger D^\mu \Phi - \frac{\lambda}{4} \left( (\Phi^\dagger \Phi)^2 - \frac{v^2}{2} \right)^2. \quad (2.10)$$

This is the canonical scalar field Lagrangian with a quartic potential and  $SU(2)_L \times U(1)_Y$ -covariant derivatives. These derivatives take the explicit form

$$D_\mu \Phi = \left( \partial_\mu \mathbb{1} - i \left( g_2 W_\mu^i T_i - \frac{1}{2} g_1 B_\mu Y \right) \right) \Phi. \quad (2.11)$$

The remarkable property of the potential term we chose is that its parameters  $\lambda$  and  $\mu$  can be chosen so as to cause the scalar field to acquire a vacuum expectation value (vev) different from zero. This non-vanishing vev breaks the  $SU(2)_L \times U(1)_Y$  gauge group spontaneously down to  $U(1)_{em}$ . The unbroken gauge group is the usual  $U(1)$  symmetry of electrodynamics.

Next, we take the vev to be of the form  $\langle \Phi \rangle = \begin{pmatrix} v \\ 0 \end{pmatrix}$  which can always be achieved by a simple rotation. This enables us to reparametrize the field to read  $\Phi = \begin{pmatrix} v + H \\ 0 \end{pmatrix} e^{i\chi}$ .  $\chi = \chi^i \tau_i$  and  $H$  represent four new real scalar fields. Making use of the left-over  $U(1)$  gauge freedom we can get rid of the  $\chi$ -field (unitary gauge). After reparametrizing the field in the Lagrangian and working out the covariant derivatives the result looks like a dogs breakfast.

The situation clears if one additionally rotates the gauge fields around the Weinberg-angle  $\theta_W$

$$A_\mu = \sin \theta_w W_\mu^3 + \cos \theta_w B_\mu, \quad Z_\mu = \cos \theta_w W_\mu^3 - \sin \theta_w B_\mu \quad \text{and} \quad W_\mu^\pm = \frac{1}{\sqrt{2}} (W_\mu^1 \mp i W_\mu^2) \quad (2.12)$$

These new fields turn out to be mass eigenstates of the gauge fields and describe physically observable particles. What happened was that the gauge fields and the Higgs field acquired mass terms through the symmetry breaking:

$$\begin{aligned} \mathcal{L}_{\text{Higgs}} = [\dots] & - \frac{1}{2} \partial_\mu H \partial^\mu H - \frac{1}{4} \lambda v^2 H^2 - \frac{1}{4} \lambda v H^3 - \frac{1}{16} \lambda H^4 \\ & - \left( \frac{1}{2} \left( \frac{gv}{2 \cos \theta_w} \right)^2 Z_\mu Z^\mu + \left( \frac{gv}{2} \right)^2 W_\mu^+ W_\mu^{-\mu} \right) \left( 1 + \frac{H}{v} \right). \end{aligned} \quad (2.13)$$

The ellipsis stands for triple and quartic gauge-interactions which appear as well since  $SU(2)$  is non-abelian. Note that the photon-field  $A_\mu$  remains massless since a  $U(1)$  subgroup of the original symmetry is unbroken. The mechanism underlying that is an analogue of the Goldstone theorem extended to local symmetries. By breaking the symmetries we do not produce massless Goldstone bosons but additional degrees of freedoms for the gauge fields. Notice that the number of degrees of freedom before and after symmetry breaking are the same. The massive gauge bosons absorbed the three of the massless fields that vanished.

The same mechanism works for generating the mass terms of the lepton and quark fields. This time we start from a massless Dirac term for the lepton singlets and doublets. We then couple the latter to the gauge fields via the covariant derivative and to the Higgs field through a Yukawa coupling including left and right-handed leptons

$$\mathcal{L}_{\text{Lep}} = \sum_k i \overline{\begin{pmatrix} \nu^k \\ l^k \end{pmatrix}_L}^T \gamma^\mu \left( D_\mu \begin{pmatrix} \nu^k \\ l^k \end{pmatrix}_L \right) + i l_R^k \gamma^\mu D_\mu l^k - \sum_{k,n} G_{kn} \overline{\begin{pmatrix} \nu^k \\ l^k \end{pmatrix}_L}^T \begin{pmatrix} \phi^+ \\ \phi^0 \end{pmatrix} l_R^n + h.c. \quad (2.14)$$

These Yukawa coupling are the only gauge invariant operators of correct mass dimension we can write down given our field content. Now we can again plug in the reparametrization of the  $\Phi$  field. Additionally we rotate the lepton fields to their mass eigenstates with the help of a couple

of unitary transformations to find

$$\begin{aligned} \mathcal{L}_{\text{Leq}} = & \sum_m \frac{g}{\sqrt{2}} W_\mu^+ \left( \overline{\mathcal{N}}_L^m \gamma^\mu \mathcal{E}_L^m \right) + \frac{g_m}{\sqrt{2}} W_\mu^- \left( \overline{\mathcal{E}}_L^m \gamma^\mu \mathcal{N}_L^m \right) - e A_\mu \overline{\mathcal{E}}^m \gamma^\mu \mathcal{E}^m \\ & + \frac{e}{s_w c_w} Z_\mu \left( \frac{1}{2} \overline{\mathcal{N}}_L^m \gamma^\mu \mathcal{N}_L^m - \frac{1}{2} \overline{\mathcal{E}}_L^m \gamma^\mu \mathcal{E}_L^m + s_w^2 \overline{\mathcal{E}}^m \gamma^\mu \mathcal{E}^m \right) - \frac{y}{\sqrt{2}} (v + H) \overline{\mathcal{E}}^m \mathcal{E}^m. \end{aligned} \quad (2.15)$$

The structure becomes clear once we define new leptonic Dirac fields  $\mathcal{E}^m = \begin{pmatrix} l_L^m \\ l_R^{m\dagger} \end{pmatrix}$  and  $\mathcal{N}^m = \begin{pmatrix} \nu_L^m \\ \nu_L^{m\dagger} \end{pmatrix}$ . Notice that there is no residue from the unitary transformations in the limit of massless neutrinos. This is in general not true.

If we try the same for the quark doublets we run into some interesting technical features. Let us start in the same way from a Lagrangian containing all possible Yukawa couplings of the quark fields to the Higgs field

$$\mathcal{L}_{\text{Quark, Yuk}} = - \sum_{m,n} G_{mn} \overline{\begin{pmatrix} u^m \\ d^m \end{pmatrix}}_L \begin{pmatrix} \phi^0 \\ \phi^- \end{pmatrix} u_R^n - \sum_{m,n} H_{mn} \overline{\begin{pmatrix} u^m \\ d^m \end{pmatrix}}_L \begin{pmatrix} -\phi^{-\dagger} \\ \phi^{0\dagger} \end{pmatrix} D_R^n + h.c. \quad (2.16)$$

As done before we can perturb  $\Phi$  about the ground state making use of the Higgs vev. The feature arises when we try to rotate the quark fields to mass eigenstates via unitary transformations. This works out perfectly fine for the interaction terms involving a Z-field just as it did for the lepton fields. The terms containing W's however pick up a non-diagonal coupling which can be summarized in the Cabbibo-Kobayashi-Maskawa-Matrix (CKM)  $V_{ij}$  defined in [8] via

$$\begin{pmatrix} V_{ud} & V_{us} & V_{ub} \\ V_{cd} & V_{cs} & V_{cb} \\ V_{td} & V_{ts} & V_{tb} \end{pmatrix} \begin{pmatrix} d \\ s \\ b \end{pmatrix} = \begin{pmatrix} \tilde{d} \\ \tilde{s} \\ \tilde{b} \end{pmatrix}. \quad (2.17)$$

The tilde indicates the interaction states. This means, that the interaction Lagrangian allows for so-called flavor-changing charged currents. As a consequence quark-flavor is in general not conserved at electroweak vertices.

The Lagrangian itself becomes

$$\begin{aligned} \mathcal{L}_{\text{Quark}} = & \sum_m \frac{g}{\sqrt{2}} W_\mu^+ \left( \overline{\mathcal{U}}_L^m V_{mn} \gamma^\mu \mathcal{D}_L^n \right) + \frac{g_m}{\sqrt{2}} W_\mu^- \left( \overline{\mathcal{D}}_L^m V^\dagger \gamma^\mu \mathcal{U}_L^m \right) \\ & + \frac{e}{s_w c_w} Z_\mu \left( \frac{1}{2} \overline{\mathcal{U}}_L^m \gamma^\mu \mathcal{U}_L^m - \frac{1}{2} \overline{\mathcal{D}}_L^m \gamma^\mu \mathcal{D}_L^m - \frac{2s_w^2}{3} \overline{\mathcal{U}}^m \gamma^\mu \mathcal{U}^m - \frac{s_w^2}{3} \overline{\mathcal{D}}^m \gamma^\mu \mathcal{D}^m \right) \\ & + e A_\mu \left( \frac{2}{3} \overline{\mathcal{U}}^m \gamma^\mu \mathcal{U}^m - \frac{1}{3} \overline{\mathcal{D}}^m \gamma^\mu \mathcal{D}^m \right) \\ & - \frac{y}{\sqrt{2}} (v + H) \overline{\mathcal{D}}^m \mathcal{D}^m - \frac{y}{\sqrt{2}} (v + H) \overline{\mathcal{U}}^m \mathcal{U}^m \end{aligned} \quad (2.18)$$

where we defined the up-type and down-type Dirac fields  $\mathcal{U}$  and  $\mathcal{D}$  analogous to the leptonic ones.

For a long time the existence of the remanent field  $H$  was unclear and disputed. With the discovery of a scalar resonance at LHC in 2012, the first step of lifting the curtain on this matter was done. The question remaining to be answered is if all the couplings are realized in nature in the way we just outlined. We will show what the best strategy is to measure them in section chapter three.

## 2.1.2 QCD

The strong interaction, which plays a leading roll in LHC-physics due to collider's hadronic nature, is gauge theory built from the remaining part of the free SM symmetry group:  $SU(3)_c$ . The eight generators  $\lambda_k$  are conventionally described by the Gell-Mann-matrices  $\lambda_k$  obeying  $[\lambda_a, \lambda_b] = f_{abc}\lambda^c$ .

We proceed in the usual manner to built a local gauge theory by taking each quark field as a  $SU(3)$  color triplet  $\Psi_f$ . The Lagrangian then takes the form

$$\mathcal{L}_{\text{QCD}} = \sum_{\text{quarks}} \bar{\Psi}_f (i\gamma^\mu D_\mu - m_f) \Psi_f - \frac{1}{2} \text{Tr}(F^{\mu\nu} F_{\mu\nu}) \quad (2.19)$$

where the last trace extends over all eight Gell-Mann-matrices. The mass parameter  $m_f$  appearing in this Lagrangian is precisely the one we introduced in the previous section through the BEH-mechanism.

This is not even marginally fitted to model real life QCD processes. An introduction to the vast field of QCD in collider physics is however beyond our scope. Since we will be dealing, for the most part, with electroweak processes and consider only parton level processes let us just mention some standard references [13] or [14] from which collider QCD can be learned.

In the end we want to verify that these theories do indeed describe physical processes. Therefore one constructs transition amplitudes  $A = \langle \text{final} | \text{initial} \rangle$  describing the probability of initial state particles scattering to certain final state ones. One usually does that by introducing the path integral over the action built from the theory above. Because this functional integral cannot be solved analytically for interacting theories one is bound to make an expansion in powers of the interaction couplings in the exponential, under the path integral. The terms in the expansion can be used calculate the Feynman rules which is done either manually or automatically using e.g. FEYNRULES.

The scattering amplitude can then be calculated using  $\langle \text{final} | \text{initial} \rangle = (2\pi)^4 \delta(P_i - P_f) i M_{fi}$  with the final and initial state momenta  $P_{i,f}$  and the matrix element  $M_{fi}$ . The matrix element is simply the sum over all contributing Feynman diagrams at a given order in perturbation theory. This is precisely the way MadGraph5 produces our amplitudes.

As a side note: If one tries to quantize such field theories as above the introduction of ghost-fields is necessary in order to make the path integral well defined. Since we are only interested in tree-level amplitudes in this work we will ignore those - their first contributions contribute at one-loop.

## 2.2 Monte Carlo Integration and Event Generation

### 2.2.1 Cross Sections and Phase Space Integrals

The transition amplitudes built from the theory presented in the last section are not good objects to observe when conducting experiments at colliders. One usually constructs an alternative quantity called the cross section. It is defined as

$$\sigma_{\text{tot}} = \frac{\text{number of transitions per unit time}}{\text{number of incoming particles per unit time, per unit surface area}}. \quad (2.20)$$

The number of transitions here means how often a certain process takes place. These quantities can be measured by counting the occurrence of particular events.

For two-to- $n$  scattering processes there exists an analytical expression for the cross section. The exact formula makes use of the squared transition amplitude  $|M_{fi}|^2$  which in turn is proportional to the transition probability. The calculation is essentially done by integrating the latter one over all of phase space. The reasoning leading to this is however not as straight forward as one



would believe including the fact that we would need to construct a Lorentz-invariant phase space measure first. This is why we only quote the final result from [15] at this point

$$\sigma_{\text{tot}} = \frac{1}{4\sqrt{(P_A P_B)^2 - m_A^2 m_B^2}} \frac{1}{(2\pi)^{3n-4}} \int \prod_{f=1}^n \frac{d^3 p_f}{2E_f} \delta^4 \left( \sum_{f=1}^n P_f - P_A - P_B \right) |M_{fi}|^2 \quad (2.21)$$

for scattering of initial states  $A$  and  $B$  to  $n$  final state particles indexed by  $f$ .

This is however not the entire truth, especially for processes at LHC. One also needs to account for the fact that at a hadron collider the initial states are not elementary particles. The fact that protons are composite particles is modeled by introducing the (experimentally measured) parton distribution functions (pdf)  $f_i(x)$ . They describe the probability of finding a particular parton (a gluon or quark) labeled by  $i$  with a certain momentum fraction  $x$  of the initial state proton's entire momentum. This assumes that the partons are collinear to the protons incident direction. A good summary of the concepts behind pdfs can be found in [14].

At this point we have to mention that the pdfs are actually not only depended on the momentum fraction  $x$  but also on the scale  $\mu_F$  at which they are evaluated. The evolution with that scale is described by the DGLAG equations proposed in e.g. [16]. For the full calculations performed here this must be taken into account. However, we suppress this dependence in our notation for now.

We can include the knowledge about the substructure of the protons by simply convolving the phase space integral (describing the hard process) with the pdf. This turns equation 2.21 into the the master formula describing the hadronic cross section at center-of-mass energy  $s$

$$\sigma_{\text{tot}} = \int_0^1 dx_1 \int_0^1 dx_2 \sum_{i,j} f_i(x_1) f_j(x_2) \sigma_{ij}(x_1, x_2, s). \quad (2.22)$$

$i$  and  $j$  are labeling the partons found in the proton while the fact that we have two distinct incident protons is reflected by the two independent proton pdfs in the integrand.  $\sigma_{ij}$  is the cross section of the hard process between the partons.

## 2.2.2 Monte-Carlo Techniques

The phase space integrals appearing in the cross section formula are not analytically solvable in almost all cases. Additionally, the pdfs are only known numerically. This means that one must resort in any case to numerical integration tools, and in particular Monte-Carlo techniques. A general pedagogical summary of the basic concepts can be found in [17]. How these techniques apply to event generators is explained in [9] and [18].

We make use of the usual way to numerically evaluate an integral. This is by evaluating the integrand at various, randomly chosen points in a small volume of the domain, multiplying the values by said small volume and summing over all volumes

$$\int_0^1 f(x) dx \approx \sum_{i=1}^N \Delta x_i f(x_i), \quad (2.23)$$

The sum becomes of course exactly equal to the integral in the limit of infinitely many points  $x_i$ , thus covering the entire integration range. Note that we limit ourselves to an integration from 0 to 1 which can always be achieved through the introduction of a suitable Jacobean  $J_1$ . Furthermore we kept the volume  $\Delta x_i$  arbitrary for every point  $x_i$ . The integration range does not necessarily need to be cut up equidistantly.

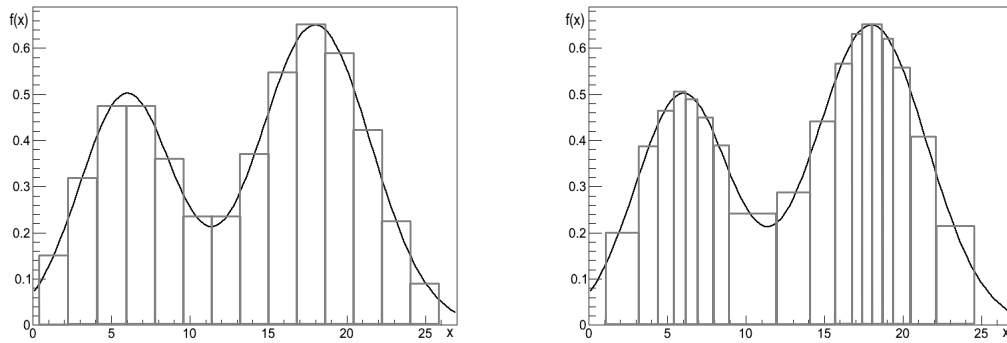


FIGURE 2.1: Visualization of conceptual idea behind importance sampling. Integration with an equidistant binning (left) e.g. Riemann integration, and importance sampling (right).

To perform an integration in  $d$  dimensions we have to trade in the random numbers  $x_i$  for random  $\mathbb{R}$ -valued vectors  $\vec{x}_i$  and the length  $\Delta x_i$  becomes a volume associated with that vector  $\Delta \vec{x}_i = \Delta x_i^1 \dots \Delta x_i^d$ . We call this volume a weight. Notice that, for a phase space integration with  $n$  final state, on-shell particles, the dimension of  $\vec{x}$  is  $(3n - 4)$  (four-momentum conservation kills four degrees of freedom!).

The problem that becomes manifest is that the variance of evaluating an integral with this approach decreases like  $1/\sqrt{N}$ ,  $N$  being the number of points with which we evaluate the integrand. With the dimensionality scaling mentioned above this becomes less than economic. One can however optimize convergence significantly by choosing the points not completely at random, i.e. by doing what is called an importance sampling. In the neighborhoods where  $f(\vec{x})$  takes larger values (for phase space integration: where there is a lot of signal) we should use a lot of points and map out the space disproportionately more than where  $f(\vec{x})$  takes on smaller values. In regions with little-to-no signal we can accordingly use a rougher sampling since statistical fluctuations here will not contribute much. Figure 2.1 visualizes the difference between the integration methods.

Implementing this importance sampling is in practice carried out by introducing an ad-hoc unknown distribution function  $g(\vec{x})$  in the following way:

$$\int_0^1 d^d x f(\vec{x}) = \int_0^1 d^d x \frac{f(\vec{x})}{g(\vec{x})} g(\vec{x}) = \left\langle \frac{f(\vec{x})}{g(\vec{x})} \right\rangle. \quad (2.24)$$

Sneaking in the distribution  $g(\vec{x})$  makes the integral become just an expectation value under  $g(\vec{x})$ . For points thrown completely at random the distribution has the interpretation of a "hit-or-miss" probability function. It tells us how probable it is for one of the randomly generated points to be accepted and to contribute to the integral. For large values of the integrand, this probability becomes correspondingly large.

The clue is to choose  $g$  in such a way that the ratio of  $f(\vec{x})$  and  $g(\vec{x})$  becomes as flat as possible. In the situation of the integrand being roughly constant, we can very well approximate the integral by calculating the average of that ratio evaluated at various points:

$$\left\langle \frac{f(\vec{x})}{g(\vec{x})} \right\rangle \approx \frac{1}{N} \sum_{j=1}^N \frac{f(\vec{x}_j)}{g(\vec{x}_j)}. \quad (2.25)$$

Note that in the case of a phase space integration the process we wish to integrate will consist of a great variety of distinct channels. In principle, a different probability distribution  $g_i(\vec{x})$  can exist for every integration  $i$  mapping out their respective channels. They are chosen in such a way that the complete probability density reads

$$g(\vec{x}) = \sum_i \alpha_i g_i(\vec{x}), \quad (2.26)$$

where the weights  $\alpha_i$  will, in general, change from iteration to iteration so as to optimize the integration. The  $\alpha_i$ s additionally have to be chosen in a way to keep the probability function correctly normalized.

Notice that the variance for our newly rewritten integral has the form

$$\text{Var}(\bar{\alpha}) = \int_0^1 d^d x \frac{f(\vec{x})^2}{g(\vec{x})}. \quad (2.27)$$

In contrast to the value of the integral itself, the variance evidently depends on how we chose the parameters  $\alpha_i$ . This is not a caveat but a feature of multi-channel integration. The parameters for every iteration are chosen in such a way that they minimize the variance. Only after this are they used to calculate the integral.

In the case of a phase space integral, this is however by far not all an event generator does. One of their main features is to translate each random number vector  $\vec{x}_i$  back to the actual four-momenta of the final and initial state particles, so in a sense it retranslates the Jacobean transformation we carried out to get a unit cube. In actuality, event generators not only calculate the cross section but also simulate physical processes, e.g. collision events. To be precise, one produces in this way only parton level processes with **MadGraph5**. To have a more realistic sample, one would still need to shower these events using e.g. **PYTHIA** [19]. Additionally, one needs to keep track of the weight associated with each phase space point, so we know the frequency with which the event occurs. This of course is given by the integrand of the phase space integral:  $J_1 |M|^2$ .

### 2.2.3 The Single Diagram Enhanced Method

**MadGraph5** runs its phase space integration using a modified version of the importance sampling. It additionally makes use of a smart decomposition of the integral and thus reduces total integration time. This decomposition draws heavily from the fact that we actually know the pole structure of what we want to integrate. The general idea is explained in [20] and [21], dating all the way to [22]. The actual algorithm used by the event generator, **MadEvent**, is described in [23].

**MadEvent** decomposes the integrand into functions that can easily be mapped by a single channel. It starts by defining a complete set of functions  $f_i$  such that

$$f(\vec{x}) = \sum_{i=1}^N f_i(\vec{x}) \quad \text{with} \quad f_i \geq 0 \quad \forall \quad i \in \{1, \dots, N\}, \quad (2.28)$$

for the function  $f(\vec{x})$  we wish to integrate. In **MadEvent**'s case  $f(\vec{x})$  is of course the matrix element and pdfs. With the help of the single channel probability functions  $g_i$ , we see that the integral actually decomposes into

$$\int d^d x f(\vec{x}) = \sum_{i=1}^n \int d^d x g_i(\vec{x}) \frac{f_i(\vec{x})}{g_i(\vec{x})} = \sum_{i=1}^n \left\langle \frac{f_i(\vec{x})}{g_i(\vec{x})} \right\rangle_i. \quad (2.29)$$

This procedure is, however, not always possible when integrating arbitrary functions. In general one has no chance of finding a basis of functions obeying these conditions. Our case on the other hand is optimal for this. The matrix-element to be integrated allows for such a decomposition if one choses the basis to be:

$$f_i = \frac{|M_i|^2}{\sum_k |M_k|^2} |M_{\text{tot}}|^2. \quad (2.30)$$

Here  $|M_i|^2$  is the squared matrix-element belonging to a single Feynman-diagram (including all that are numerically equal) and  $|M_{\text{tot}}|^2 = |\sum_k M_k|^2$  is the total amplitude squared.

The pole-structure of the single  $M_i$  is well known and derived from the form of the propagators (Breit-Wigner, etc). This procedure is known as the multi-channel single diagram enhanced

method. So what `MadGraph5` does in the end is nothing but decompose its phase space integral into various channels with known mappings. Notice that `MadGraph5` choses which diagram to integrate at random - depending on the fraction the channel contributes to the total cross section. The numerically evaluated amplitudes is then reweighted accordingly. So in a sense, it does a double importance sampling. As smart this procedure is it will become the major concern for our endeavor.

The single diagram enhanced method has several computational advantages over the usual integration algorithms when addressing to cross sections.

- When we split up the matrix element into simple functions, we split up the phase space integral into single integrations. The complexity of integrating these single integrals is setting the complexity of the entire integration procedure. Even if we increase the number of channels or the difficulty of the process, the single integrals we combine in the end remain at the same difficulty. Subsequently the integration time is limited only by the number of sub-integrals; while in the full integral an increase in complexity of the function can elongate the integration time immensely.
- The splitting of phase space integrals is largely uncorrelated. We can evaluate them independently making use of additional internal processors or other external capacities. Such a parallel integration is, in general, not possible in the head-on approach.
- All channels are equally, carefully mapped in the classical approach, no matter how much they contribute to the final result. With a simple reweighing (introducing weights  $\beta_i$  analogously to the  $\alpha_i$ ) and choosing  $\beta_i = \frac{I_i}{T}$  with  $I_i$  being the cross section for channel  $i$ , we save time by only spending effort on parts that actually contribute. The weight then determines how many points we actually have to use for mapping the channel.
- Lastly we are in the situation where one is able to regroup and categorize integrals by their similar pole structure - thus saving even more time.

## 2.3 The Log-Likelihood Analysis

We now focus for a moment on the mathematical methods needed for `MadMax`. In this section we review the theoretical background underlying the tool we constructed and describe in this thesis. How the Monte Carlo methods relate to the log-Likelihood analysis is described in [24].

### 2.3.1 Exclusion Limits

Imagine at the LHC that a bunch of  $\mu^+\mu^-$  pairs are produced and that the invariant masses of these pairs are somewhat close to the Higgs mass. Are these actually Higgs decay products or just random particles that happen to derive from particles with kinematics mimicking a Higgs? How many muon pairs do we need to observe before we can meaningfully conclude what it is we are observing?

Luckily there are distinguished statistical ways and techniques of answering these questions. An excellent review of the techniques used is given in [25] or with a focus on LHC Higgs discovery in [26], [27]. A procedure on how to automatize these procedures, can be found for LHC physics in [28].

Addressing our question first one needs to understand it is we are actually looking at. The events recorded by a detector are data that are described by a probability distribution. This distribution in turn is solemnly characterized by a set of parameters, which are a priori unknown to us but have in general fixed values. This could for example (and for all practical purposed it is) be a Poisson distribution which is determined by its median.

In the following, we shall denote the set of parameters by  $a$  and our data i.e. the events recorded

by  $x = \{x_1, x_2, \dots, x_N\}$ .

Now to formalize our question from earlier, we introduce the so-called hypothesis test. We stipulate that there are two explanations of what we observe and call them hypotheses. In the  $H \rightarrow \mu^+ \mu^-$  example, one hypothesis would clearly be "some of the muons come from decaying Higgs bosons". We call this hypothesis assuming signal plus background  $H_1$ . In the complementary explanation would be that all muons are coming from other electroweak processes not involving a Higgs. This represents a null or background-only hypothesis named  $H_0$ .

If the events are produced by a Gaussian distribution for signal and background-hypothesis, it is straight forward to quantify an excess. For a certain event count, we can give the probability that the background will result in a particular distribution. We can give the number of standard deviations,  $\sigma$ , for this probability. This is simply the distance the measured count is away from the expected background median. For example  $5\sigma$  would correspond to a probability of  $p = 0.000006$ . If a hypothesis in particle physics is excluded at  $5\sigma$  we can claim discovery of the signal. The probability for a background distribution to produce the measurement must be smaller than this value. Only if this happens we can claim the background-only hypothesis to be invalid. This is one of the philosophical problems of physics: verification is per se not possible. Because of that, the only way possible to make a discovery is by excluding everything else (at least up to a certain probability).

In general do the event distributions for the hypothesis not follow Gaussians distributions. Neither is it always wise to take the event count as the discriminating variable on which we base our discovery. The rules however remain the same. We define the so-called background confidence level  $CL_b$  as

$$CL_b = \int_{q_0}^{\infty} dq \rho_b(q), \quad (2.31)$$

which tells the probability of observing the value  $q_0$  of some variable under background-only hypothesis.  $q$  is called the test statistic and can be almost any quantity described by the events. For conventional reasons we can convert this number to Gaussian standard deviations in a canonical way (cf. e.g. [29]).

$$CL_b = \frac{1}{2} - \frac{1}{\sqrt{\pi}} \int_z^{\infty} dx e^{-\frac{x^2}{2}}, \quad (2.32)$$

which implicitly defines the number of standard deviations  $z$  for a given confidence limit  $CL_b$ . If we solve for  $z$  we found the confidence level in standard deviations what is usually the final result published - regardless of what distribution one is actually dealing with.

### 2.3.2 The Maximum Likelihood Method

If we would know the analytical form of the probability distributions  $\rho$  underlying our events as mentioned above (a different one for each hypothesis) we could say which theory is more probable and even how much more probable! But since at least the true values of the parameters determining the shape are inaccessible, we have to help ourself differently.

The probability of observing a certain event  $x_i$  we denote by  $f(x_i|a)$ , so that the probability to observe the full sample is given by

$$F(x_1, x_2, \dots, x_N|a) = \prod_{n=1}^N f(x_n|a). \quad (2.33)$$

This factorization is of course only possible if one assumes no correlation between the events, which we did.

The Likelihood-function in turn is then defined as

$$F(x_1, x_2, \dots, x_N|a) = \prod_{n=1}^N f(x_n|a) = \prod_{n=1}^N l(x_n|a) = L(a|x_1, x_2, \dots, x_N) \quad (2.34)$$

Note: For fixed  $x$  and  $a$  the Likelihood and the probability distribution do numerically coincide. The probability distribution however must be read as a function in "x", i.e. the probability to actually produce the given data set, while the Likelihood is a function in  $a$ , determining how likely (hence the name) a hypothesis is under the assumption that  $x$  was measured. The Likelihood is not a probability function - therefor one can only make statements relative to Likelihoods of other hypothesis.

Neyman and Pearson [30] showed that the best way to compare Likelihoods is to look at their quotient. In this context best means that it produces the lowest chance of committing a Type I or Type II error. A Type I error occurs when the null hypothesis  $H_0$  is true but rejected anyhow. On the other hand Type II occurs when the hypothesis is false but accepted. A schematic way of how to visualize the comparison between Likelihoods can be found in Figure 2.3.2.

$$Q = \frac{L(x_1, x_2, \dots, x_N | H_0)}{L(x_1, x_2, \dots, x_N | H_1)}. \quad (2.35)$$

The quotient serves us as the test statistic in our hypothesis test from now on. In our case we would consider the signal+background over the background-only hypothesis.

The Likelihoods for these two hypothesis are given by

$$\begin{aligned} L(x_1, x_2, \dots, x_N | H_1) &= \left( \frac{e^{-(s+b)}}{N!} (s+b)^N \right) \times \prod_{i=1}^N f_{s+b}(x_i | a) \\ L(x_1, x_2, \dots, x_N | H_0) &= \left( \frac{e^{-b}}{N!} b^N \right) \times \prod_{i=1}^N f_b(x_i | a) \end{aligned} \quad (2.36)$$

where the product extends over  $N$  independent events. Since we are dealing with a number counting experiment the probability to observe a certain number of events is given by the Poisson distribution in the first term, while the product runs through all the single events's Likelihoods. The parameters  $a$  used in the definition 2.34 are essentially the expected event counts. For each Likelihood we have  $a_1 = s + b$  and  $a_2 = b$  respectively.

For calculation reasons one usually considers the natural logarithm of the Likelihood:

$$\begin{aligned} q(x) &= \log Q(x) \\ &= -s + \sum_{n=1}^N \log \left( \frac{s+b}{b} \frac{f_{s+b}(x_n)}{f_b(x_n)} \right) \\ &= -s + \sum_{n=1}^N \log \left( 1 + \frac{s f_s(x_n)}{b f_b(x_n)} \right) \end{aligned} \quad (2.37)$$

In the last term we assumed that the signal+background distribution can be decomposed as

$$f_{s+b}(x) = \frac{s f_s(x) + b f_b(x)}{s + b}. \quad (2.38)$$

Such a factorization is only possible if signal and background only distributions are not interfering.

In our case we can construct the probability density functions directly from the matrix elements of the processes under consideration. They are essentially given for every event by the differential cross section evaluated at the point in phase space belonging to that event.

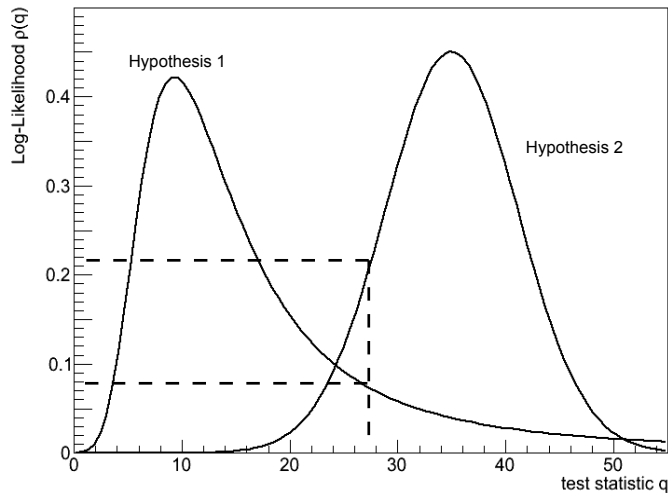


FIGURE 2.2: Log-Likelihood distributions for different hypothesis. We see that for a given value of the test statistic  $q$  (dashed lines) the likelihood of hypothesis 2 to be true exceeds the one of hypothesis 1.

Noting that the expected number of events under each of the hypothesis is given through  $s = \mathcal{L} \times \sigma_s$  and  $b = \mathcal{L} \times \sigma_b$  respectively we can rewrite our expression for the log-likelihood as a function of the random number vector.

Assuming that the phase space is mapped by a vector of random number  $\vec{r}$  we can write them down as  $f_s(\vec{r}) = d\sigma_s(\vec{r})/\sigma_s$  and  $f_b(\vec{r}) = d\sigma_b(\vec{r})/\sigma_b$ . The division by the total cross sections accounts for a proper normalization of the distributions.

This function finally assigns to every point in phase space its corresponding log-likelihood.

$$\begin{aligned} q(\vec{r}) &= -\sigma_s \mathcal{L} + \log \left( 1 + \frac{\mathcal{L} \sigma_s}{\mathcal{L} \sigma_b} \frac{d\sigma_s(\vec{r})}{\sigma_s} \frac{\sigma_b}{d\sigma_b(\vec{r})} \right) \\ &= -\sigma_s \mathcal{L} + \log \left( 1 + \frac{d\sigma_s(\vec{r})}{d\sigma_b(\vec{r})} \right) \end{aligned} \quad (2.39)$$

In order to find out which regions of phase space are worthwhile investigating we need to find a probability distribution in  $q$ . We start by constructing single-event distributions from the phase space weights of the events. Under the background-only hypothesis this is easily done via

$$\rho_{1,b}(q_0) = \int d\vec{r} \frac{d\sigma_b(\vec{r})}{\sigma_{\text{tot},b}} \delta(q(\vec{r}) - q_0), \quad (2.40)$$

and of course completely analogous for the signal hypothesis.

We need to deal with a lot of events in our analysis. The best way to do this is to successively apply the single-event distributions. In order for two events to happen a single one must happen first. In general to get from a  $N - 1$  distribution to  $N$  distribution simply convolute the  $N - 1$  distribution with the single-event one. So in the end one finds  $N$  convolutions of the single-event distribution with itself.

The resulting convoluted integrals can be carried out numerically again using Monte Carlo methods [31]. Alternatively one can use a simple Fourier transform and manipulate the terms a little bit first. This is originally found in [32]. One is then left to numerically evaluate the Fourier transform. Since this is quite cumbersome for infinitely many events to evaluate we use LEPStats4LHC described in [33]. It is based on the Fastest Fourier Transform in the West (FFTW) [34]. The manipulations mentioned are fairly straight forward. In Fourier space a convolution turns into a simple multiplication, which tempts us to write the  $N$  convolutions as



a  $N$ th power of

$$\rho_b(q) = \sum_{n=1}^{\infty} \left( e^{-b} \frac{b^n}{n!} \right) \rho_{n,b}(q). \quad (2.41)$$

Now to make use of the fact that  $\mathcal{F}(\rho_{n,b}(q)) = \mathcal{F}(\rho_{1,b}(q))^n$ . We double Fourier-transform the  $n$ -event distribution

$$\begin{aligned} \rho_b(q) &= \mathcal{F}(\mathcal{F}(\rho_b(q))) \\ &= \mathcal{F} \left( \sum_{n=1}^{\infty} \left( e^{-b} \frac{b^n}{n!} \right) (\mathcal{F}(\rho_{1,b}(q)))^n \right) \\ &= \mathcal{F}(\exp(b(\mathcal{F}(\rho_{1,b}(q)) - 1))). \end{aligned} \quad (2.42)$$

In the first step we the linearity of Fourier-transforms was exploited and then we identified the Taylor expansion of the exponential function. The entire strategy is summarized in [29] with an focus on how to automatize these calculations given a one event distribution.

Following exactly the same reasoning for the signal plus background hypothesis we can find the  $s+b$ -distribution

$$\rho_{s+b}(q) = \mathcal{F}(\exp(b(\mathcal{F}(\rho_{1,b}(q)) - 1) + s(\mathcal{F}(\rho_{1,s}(q)) - 1))). \quad (2.43)$$

With those handy tools ready the only task left is to get the single-event distributions from a event generator.

### 2.3.3 On the Way to MadMax

The single diagram enhanced method requires **MadGraph5** to evaluate its cross sections point wise. Integrating a Log-Likelihood function in the way described previously should be straight forward. The idea would be to have it calculate the distribution according to equation 2.40 instead of the pure integrand. This of course requires that after a phase space point is found all signal and background matrix-elements are ready to be evaluated at that point.

The idea is to have **MadGraph5** not only give out the four-momenta of each event it considers, but also the corresponding Likelihood for that point according to equation 2.39 and the value of the probability density  $\rho_{1,b}(q)$ . These values we can then turn into a histogram counting how often which Likelihood value appears. That way we would get a numerical expression for the single-event iLikelihood distribution.

With the help of **LEPStats4LHC** we can turn this distribution into the multi-event distribution desired. This is done in strict accordance with equation 2.42. From that distribution we would finally be able to calculate the significance of the signal over the background with one last numerical integration. This result can then be converted into Gaussian standard deviations. The so found significance is the maximum expected significance. It serves as an upper limit in signal searches not to find discriminating variables or clever cut strategies.

With the event file containing the Log-Likelihood for every event we can take it even one step further. We can build a histogram from the event file showing how the Likelihood is distributed with a kinematic variable of our choice. These distributions tell us precisely what we want to know: In which parts of phase space is the significance of the signal over the backgrounds actually picked up. This enables us to differentiate between phase space regions suitable for say a Higgs search and those negligible.

As usual this is easier said than done. The problem lies in the fact that **MadGraph5** is based on the single diagram enhanced technique. It does not actually calculate its full integrand but chops it up and calculates the pieces. It does not evaluate the full matrix element but only contributions from single diagrams which it then reweighs. We on the other hand want to calculate the integral over a logarithm which makes such decomposition impossible. The only way to deal with that is to take the matrix elements generated by **MadGraph5**, which are still perfectly fine and set up our own integration routines. Only in that way we can capture the structure of the



entire matrix element needed for the Likelihood.

Although `MadGraph5` becomes very efficient through the single diagram enhanced method it is almost useless to compute integrals over any other functions. To implement a likelihood computation we are essentially forced to mimic everything `MadGraph5` does to its matrix elements after the generation of the phase space points.

We will explain that the subroutine `auto.dsig` evaluates the integral

$$\sigma_{\text{tot}} = \int d\text{LIPS} d\sigma(p) \quad (2.44)$$

for a given phase space point by choosing the diagram of a random subprocess (`dsig1`, `dsig2`,...) which is then weighted. The differentials `dsig` are essentially the products of the squared matrix elements and the parton density functions. The pdf (in our case `Cteq6l1`) is read out directly from file while the helicity amplitude for the matrix element is calculated by the `HELAS` routines. We can work with both objects largely unaltered.

The random choice is based on the contribution of the subprocess to the total cross section. This is the realization of the single diagram enhanced method and follows precisely equation 2.30 describing the decomposition.

Our goal is to find the Likelihood distribution which is done by evaluating

$$q(p) = -\sigma_{\text{tot}, s} \mathcal{L} + \log \left( 1 + \frac{d\sigma_s(p)}{d\sigma_b(p)} \right) \quad (2.45)$$

at every phase space point. For this the full differential  $d\sigma$  must contain all subprocesses for both signal and background.

## Chapter 3

# From MadGraph to MadMax

### 3.1 The Integration routines in MadGraph5

In this chapter we will describe how **MadMax** works in details. Before explaining how the concepts outlined in the last chapter can be realized one needs to understand how **MadGraph5** itself does the integration. Only after seeing how the single diagram enhanced method works in the original program we are in the position to find the spot in which **MadMax** needs to be implemented.

Figure 3.1 shows the essential parts of the main integration routine of **MadGraph5**. We highlighted the point at which **MadMax** is incorporated.

Before we start describing the integration algorithm in **MadGraph5** we must be clear on the terminology. An entire process integrated consists of subprocesses it added up. The subprocesses have physically well distinguishable final- or initial-states. It becomes necessary in **MadMax** to label these. We will do this with the letters  $a, b, \dots$ . Furthermore will different processes be labeled with  $n$ .

Each of the subprocesses consists of sub-diagrams having the same external particles. Over these we sum coherently. The matrix elements for the sub-diagrams we will label  $i, j, \dots$ . The main integration routine of **MadGraph5** is *sample\_full*. It is the top level routine called by the driver of the program. It coordinates all the subprocesses necessary to compute the cross sections. This is the routine that needs to contain the *madmax* routine in the end. At any other point we do not have a chance to get all the information needed to mimic everything done by **MadGraph5**.

The first task is to get the phase space points for which we want to evaluate the matrix elements. *sample\_full* acquires them by first invoking *x\_to\_the\_f\_arg*. This particular subroutine located in *genps.f* has two tasks. Firstly it activates the random number generator through the routine *sample\_get\_x*. The Monte Carlo generator produces a random number vector  $x$  and the corresponding weight  $WGT$  which are then further processed. This is necessary since both are only defined on the unit cube.

In a second step the random number vector and its weight are transformed by *x\_to\_the\_f\_arg* to the four-momenta  $p$  of the event and the corresponding phase-space weight  $wgt$ . The transformed vector and weight are already the correct arguments for the matrix elements. Both are returned to the main integration routine.

Before reaching the matrix elements the four-momentum  $p$  has to pass the kinematic cuts. In the routine *passpoint*, which is located in *cuts.f* it successively is tested for all cuts set in the *run\_card.dat*. Additionally all relevant couplings and scales are set while doing so. Both the couplings and the scales must be reproduced for **MadMax** since the amplitudes depend on them.

With the phase space point and its volume present it is time to generate the matrix elements. The integration routine calls for this reason *auto\_dsig*. The subroutine first calculates the necessary symmetry factors and crossings needed. Afterwards it randomly choses a diagram to evaluate. At this point the single diagram enhanced method is realized. Choosing just one of

the diagrams and reweighing is nothing but the decomposition

$$f_i(p) = \frac{|M_i|^2}{\sum_j |M_j|^2} \left| \sum_j M_j \right|^2. \quad (3.1)$$

$M_i$  is the amplitude for a single diagram of which we know the pole structure. The squared sum over all these amplitudes is then evidently the total transition probability for a given subprocess. If a process consists of various subprocesses which are not added coherently **MadGraph5** carries out the same integration mechanism for each one separately and combines them in the end.

All the squared diagrams  $|M_i|^2$  for the process are collected and stored in the subroutines *dsig1*, *dsig2*,... . Those matrix elements contain essentially the product of their squared helicity amplitudes and the pdfs. The helicity amplitudes are generated by the underlying HELAS routines described in [35]. The way they are realized and implemented in **MadGraph5** is found in [36].

Based on its relative contribution to the the partial cross section one of the little *dsigs* is chosen at random. The random number routine who does this is called *ranmar*. The weighted random choosing makes sure that the channel with the highest contribution to the cross section is mapped most accurately.

Each of the so found evaluated matrix elements is then sent back to the main integration routine. At that point we are finally able to incorporate **MadMax**. The main routine for our program, named *madmax*, receives the four-momentum and weight used by *sample\_full*. We chose to implement our main routine here because after the matrix elements have been evaluated by **MadGraph5** all subroutines are initialized and all parameters have been loaded. They can now immediately be used by us.

The main integration routine on the other hand essentially finishes its run by storing the result via the subroutine *sample\_put\_point*. After this it essentially starts over again. When the last phase space point of the last iteration has been calculated it combines all the partial cross sections to get the full result which is then given to the output.

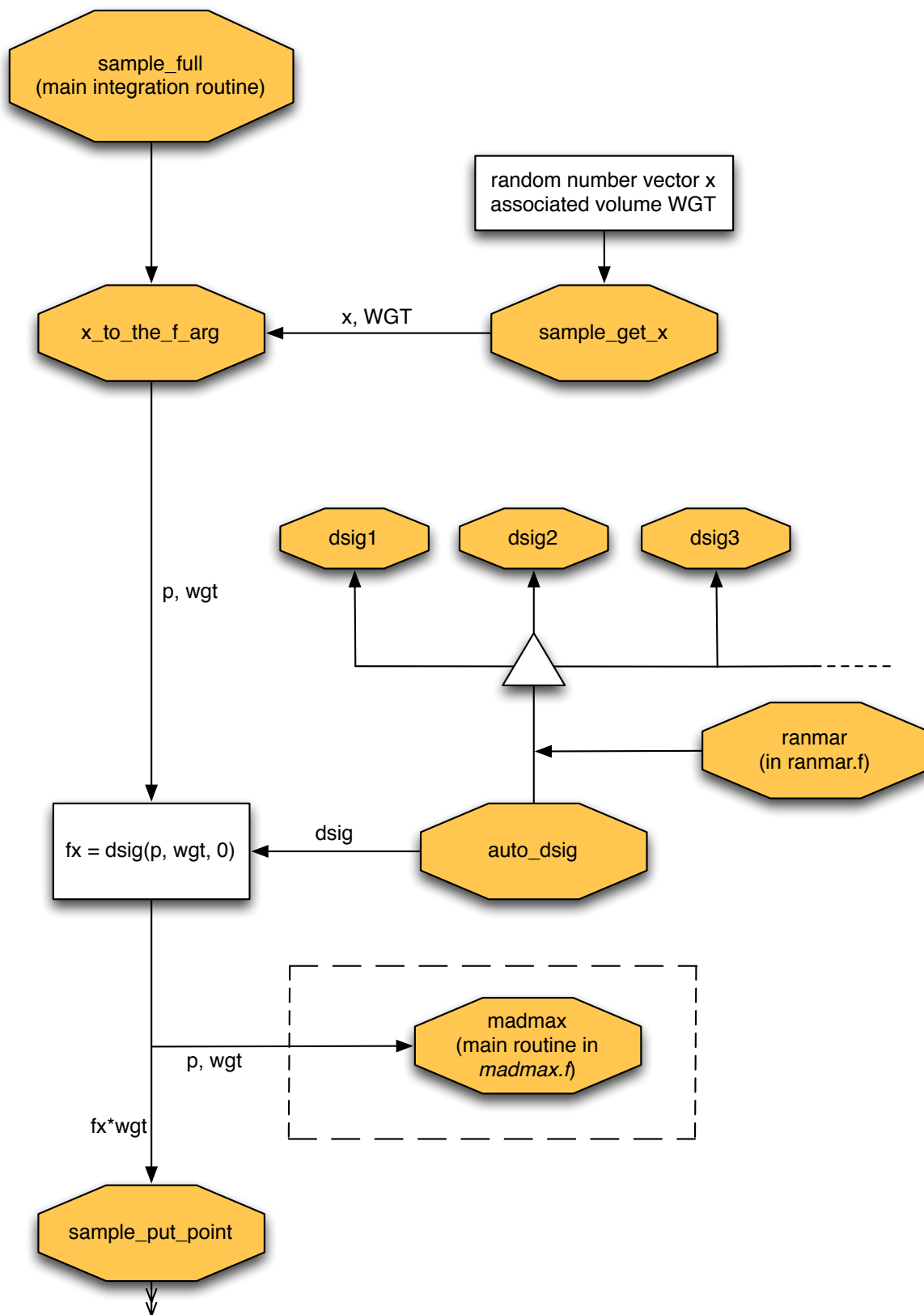


FIGURE 3.1: Flow-chart for the schematics of the important part of the main integration subroutine `sample.full` of `MadGraph`. The arrows represent calls of other subroutines and the label their corresponding handover values. The main purpose is to visualize the point at which `MadMax` is implemented into the integration routine.

## 3.2 Construction and Implementation

After we found out where the best place is to set the *madmax* routine we can explain how it realizes the modified single diagram enhanced method. With the help of our method we are not only able to reproduce the full cross sections MadGraph5 computes but also to do calculate the log-Likelihood functions described in chapter 2. Figure 3.2 shows the schematics of the main routine of MadMax.

Every time *sample\_full* produces a new phase space point it calls the *madmax* routine and hands over its current four-momentum  $\vec{p}$  and weight *wgt*. Just like the original main integration routine we built ours from different blocks called successively.

The initialization *madmax\_initialize* is only invoked for the first time the routine *madmax* gets called by *sample\_full*. Its task is it to import all the names and paths of the subprocesses that are actually part of the signal and background processes. These are precisely the subprocess folders generated by MadGraph5 in the first place. The information needed to call the subprocesses has been stored in the file *madmax\_processes.dat* when the folders were set up. They are of course independent and unrelated for the signal and background integrations.

The main part of the routine runs every time i.e. for every phase space point coming through it. It consists of two successive computations. After determining in which subprocess folder we are (which is important since the four-momenta are optimized to map that particular subprocess) the integration loops start. We loop over all signal channels and call a new program named *get\_dsig* for every single one.

This external program receives the four-momenta, weights and external parameters through a pipe - that is by essentially storing them intermediately. It first calculates all necessary couplings and scales by calling on *passcuts(p)* just the same way the main integration routine in MadGraph does. For this to work all the routine needs to have is the center of mass rapidity which we calculate from scratch externally. It also requires the Bjorken scaling variable  $x$  which we import from the main integration routine together with the four-momenta and weights.

A word about those couplings. We need to work with fixed renormalization and factorization scales  $\mu_R$  and  $\mu_F$ . The integration extends over many different processes some of which contain heavy intermediate particles others do not. In this scenario a dynamical scale cannot be implemented in a meaningful way. It is however still necessary to calculate the couplings in the cut routine. Not only do these routines calculate the values of the couplings but more importantly their structure. Especially for the various gluon couplings it turns out that there are a lot of non negligible complex factors.

The program additionally takes care of all symmetry factors and momenta switches which are necessary to avoid over-counting (e.g. s and t-channels of the same diagram are treated simultaneously while switched initial states are counted twice).

In the end *get\_dsig* is able to call the single diagram routines *dsig1*, *dsig2*,... which we do not chose at random and reweigh as opposed to what MadGraph does. We calculate all of them, add them up and get our subprocess  $d\sigma$  that way. This follows a modified single diagram enhanced method given through

$$f_i(p) = \frac{|M_{ia}^n|^2}{\sum_{jbm} |M_{jb}^m|^2} f(p). \quad (3.2)$$

The index  $i$  labels the single diagrams we consider.  $a$  counts the subprocesses which we need to combine in the end. For the case of more than one signal or background processes we also have to label those (and add them up) - that is the remaining index  $n$ .

This replaces the decomposition MadGraph5 does given in equation 3.1.

The so found *dsig* contains the information of the full amplitude and is then shipped back to the *madmax* routine via a pipe.

The same thing happens for all the background processes chosen. They of course invoke their own copies of *get\_dsig* but these are structurally equivalent to the signal ones.

Now we can add up all the  $d\sigma$ 's and that way reproduce the total cross section (at least for that particular subprocess folder) MadGraph would. Our top level loop sums up all subprocesses for all signal and all backgrounds. That way we produce the total cross sections.

Since our integration is parallel in nature we get out both the signal and background cross sections at the same time. Additionally we are also in the position to calculate any function in the integrand of the phase space integral since we have the complete differentials. This is the virtue of our modified single diagram enhanced method.

To calculate any function of the matrix element we implemented the routine *madmax.function*. In our particular case it calculates the Likelihood defined in equation 2.45.

With the final event passing through the *madmax* routine the output routines are then called. They summarize the run and print the results.

This is namely done by *madmax.summarize\_run* and *madmax.print\_results*. The first one combines the partial cross sections calculated and stored for every phase-space point and every subprocess. They are all combined to give the full cross sections for signal and backgrounds. Afterwards these are printed as results.

After the parallel integration is done we built in a backdoor for the Likelihood project called *madmax.loglikelihood*. Its a routine that can call on an automatized version of LEPStats4LHC. That way we automatically do the calculation of the  $n$ -event likelihoods from the single-event ones calculated by MadMax. Both distributions are then returned to the user as final results. Additionally we get out the Gaussian significance of the signal over the background.

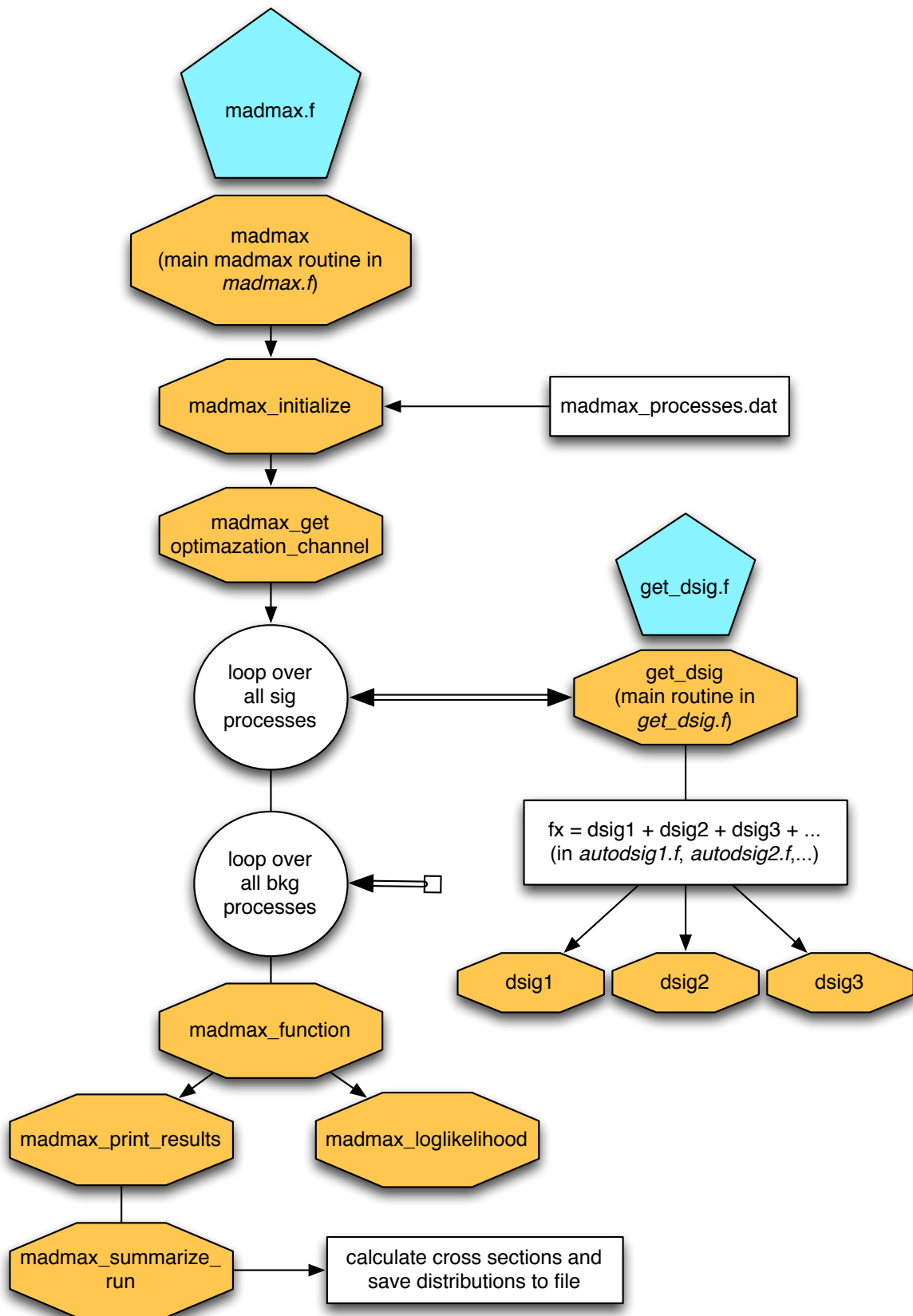


FIGURE 3.2: Flow-chart for the schematics of MadMax as it is called in the main integration routine of MadGraph. The double arrows represent the exchange of the integration in and output via a pipe. Note that the background loop is linked in the same way to its own `get_dsig` as the signal loop. We omit it here for transparency reasons.

### 3.3 Control of the MadMax Results

The question we have to deal with next is if the concepts underlying MadMax actually work and if they are realized in our program correctly. The way we check this proceeds in two steps.

First in order to control if all the differential cross sections are calculated correctly we make MadMax and MadGraph5 integrate a process with only one diagram (e.g. electron positron to muon and antimuon with only a photon exchanged). That way the single diagram enhanced method is forced to chose the same diagram every time and we can check if the numerical values coincide pointwise with the ones we calculate. The so found `dsigs` have to coincide to the last digit. If that is the case we know that we supply everything that is needed to calculate the matrix elements.

In the very same manner we integrate appropriate processes to test if the pdfs, the symmetry factors and all other details are correctly working as well. The results for these analysis can be found in appendix A.

The total cross section of an entire subprocess we check in the next step. When doing this one of the structural weak points of our original integration method becomes evident. All results point to the fact that we reproduce the signal cross sections fairly accurate. Since we are using the same four-momenta that MadGraph optimized for that very process there is no reason that this should not be the case.

The background cross sections are however not produced correctly by the parallel integration. The four-momenta are optimized to map out the phase space of the signal process which means they reflect the pole structure of the signal matrix element. The background, in general, has a completely different structure. If one goes to the limit of infinitely many points both cross sections of course converge to the true values because then all of phase space is mapped with the same accuracy. We solved this problem by by our modified diagram approach which enables us to combine signal and background optimized four-momenta.

	No. events	$pp > h > jj$	$pp > za > jj$	$pp > g > jj$
Optimization	Mg5	$(0.0265 \pm 0.0004)$ pb	$(1.33 \pm 0.01) \times 10^5$ pb	$(8.3 \pm 0.07) \times 10^8$ pb
signal	1000	$(0.0264 \pm 0.02)$ pb	$(0.81 \pm 0.6) \times 10^5$ pb	$(6.42 \pm 5.0) \times 10^8$ pb
	10000	$(0.0265 \pm 0.004)$ pb	$(1.07 \pm 0.2) \times 10^5$ pb	$(7.93 \pm 0.9) \times 10^8$ pb
	100000	$(0.0265 \pm 0.002)$ pb	$(1.30 \pm 0.05) \times 10^5$ pb	$(8.12 \pm 0.2) \times 10^8$ pb
background	1000	$(0.0149 \pm 0.03)$ pb	$(1.29 \pm 0.3) \times 10^5$ pb	$(7.94 \pm 2.1) \times 10^8$ pb
	10000	$(0.0210 \pm 0.01)$ pb	$(1.30 \pm 0.1) \times 10^5$ pb	$(7.92 \pm 0.3) \times 10^8$ pb
	100000	$(0.0259 \pm 0.002)$ pb	$(1.30 \pm 0.05) \times 10^5$ pb	$(8.11 \pm 0.2) \times 10^8$ pb
signal and background	1000	$(0.0244 \pm 0.02)$ pb	$(1.27 \pm 0.4) \times 10^5$ pb	$(7.62 \pm 2.7) \times 10^8$ pb
	10000	$(0.0249 \pm 0.007)$ pb	$(1.28 \pm 0.3) \times 10^5$ pb	$(7.88 \pm 0.4) \times 10^8$ pb
	100000	$(0.0250 \pm 0.004)$ pb	$(1.28 \pm 0.07) \times 10^5$ pb	$(8.12 \pm 0.2) \times 10^8$ pb

TABLE 3.1: Proton collision producing two jets - Higgs vs electroweak and QCD poles. We see how the optimization procedure and the statistics dictate the accuracy of the cross section.



The advantages of each method are seen when running an example. We investigate a simple hadronic process: two colliding protons produce two final state jets. In the signal process this is done via an intermediate Higgs. The backgrounds we take to be (i) purely electroweak without a Higgs and (ii) a purely QCD one. Our processes exhibit three different pole structures - a pure Breit-Wigner pole for the Higgs, a pure  $1/s$  structure for the QCD process and a mix for the intermediate photon and weak bosons. The results are summarized in table 3.1

By looking at the cross sections we see the difference between the methods. When optimizing on the signal or background processes alone we can produce accurate cross sections for either one. For a combined optimization we map all the poles of all processes but lose accuracy due to our limited event number. Notice how all the results improve as we increase the statistics.

For this simple two-to-two process the differences are all still within reason for either method. Once we go to more complicated processes however we see that the cross sections are wrong by orders of magnitude.

Our goal is it to calculate the Log-Likelihood functions with maximal precision. Therefore we chose the combined optimization in order to map the correct pole structure. The pole structure is vital to our calculation since it determines where the integrand containing the logarithm takes large values.

The only way to carry out the integration more accurately would be to use four-momenta optimized on the integrand containing the entire logarithm itself. This can not be done using the single diagram enhanced method since it relies on the additivity of the integrand. We will see in the next section that we already are in good agreement with our benchmark process using our method.

## 3.4 Higgs-production in WBF and successive decay to a $\mu^+\mu^-$ pair

### 3.4.1 The Process

Let us finally turn to a more realistic application of our new tool. As mentioned is the understanding of the Higgs couplings to the Standard Model particles one of the main focuses of modern research. To learn more about these couplings one must produce processes containing the ones of interest. A comprehensive list of the discovery channels and their advantages and disadvantages can be found in [37].

We chose to investigate Higgs production in weak boson fusion with a successive decay of the Higgs to a  $\mu^+\mu^-$  pair. A Likelihood analysis of the process for LHC is presented in [38]. We take the results from the paper as a benchmark for MadMax.

The process neither contains the dominating production channel for the SM-Higgs nor one of its dominating decay channels. It has been established that Higgs production through gluon fusion is the largest contributor for Higgs production at the LHC. An analysis for our decay with a Higgs coming from gluon fusion can be found in [39].

Higgs bosons produced in WBF are however especially appealing since this process is directly sensitive to the  $VVH$  gauge couplings described in equation 2.13. The structure of the gauge couplings is one important aspect that needs experimental confirmation. Through the application of suitable cuts is the channel well distinguishable from gluon fusion.

The dominating leptonic branching ratio for the Higgs is for its decay to tau lepton pairs  $\tau^+\tau^-$ . We wish however to ultimately examine the Yukawa couplings to all lepton generations. Therefore it is important to not only probe the tau lepton coupling but to check the couplings to the lighter generations. That way we can find out if all couplings scale with their mass the way equation 2.15 predicts. The decay to  $\mu^+\mu^-$  is on the other hand easier to observe since unlike the  $\tau$  the  $\mu$  does not decay hadronically.

We also chose WBF and a subsequent decay to  $\mu^+\mu^-$  since it is the perfect playground for our new tool. It exhibits very small signal rates and thus is hard to distinguish from the irreducible backgrounds. Furthermore are there hardly any distinct kinematic features that help us

to apply a smart cut analysis.

The irreducible backgrounds are purely electroweak and the corresponding QCD process. Figure 3.3 shows a representative Feynman diagram for the signal and each of the backgrounds. All other backgrounds mimicking the signal (e.g.  $W^+W^-$  and two jets with the neutrinos from the  $W$  decay being aligned appropriately) are either suppressed right away or kinematically so different that the cuts in appendix A.1.3 take care of them.

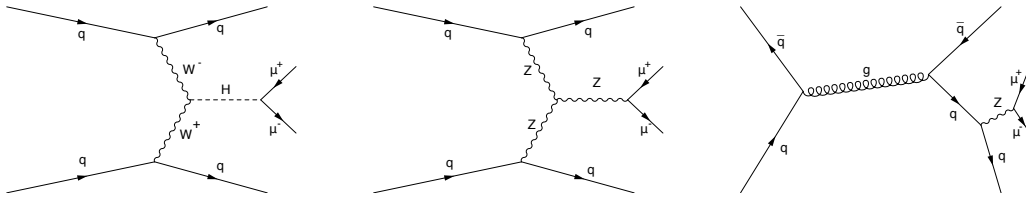


FIGURE 3.3: Representative Feynman diagrams for the signal and the backgrounds. We have Higgs production via wbf (left), the purely electroweak background (middle) and the QCD background (right).

The specific set up we adopt from [7], which also presents the results we are trying to reproduce as a benchmark. A detailed description of how the signal and the background have to be set up in MadGraph5 is found in the appendix A.1.1.

### 3.4.2 Detector Effects

The natural Higgs width of  $\Gamma_H = 4.22 \times 10^{-3} \text{GeV}$  of a 126GeV Higgs we calculated in the appendix is much smaller than the detector resolution of any LHC experiment. For this example we chose the resolution to be 1.6GeV for CMS in accordance with the original paper.

The distribution of the invariant mass of the muon pairs follows a Breit-Wigner shape with width  $\Gamma_H$  if no detector effects are included. The form derives directly from the form of the exact propagator for a scalar. In MadGraph5's conventions the propagator is defined as

$$G_{\text{BW}}(|p|) = \frac{ig_H}{p^\mu p_\mu - m_H(m_H - i\Gamma_H)}, \quad (3.3)$$

where  $g_H$  represents a coupling constant absorbed in the Breit-Wigner definition.

We wish to account for the finite experimental resolution at least to some degree. To this end we convolve the narrow Breit-Wigner propagator for the Higgs with a much more washed out shape. A convenient choice for this shape is an appropriately chosen Gaussian distribution.

Through a simple trick we can get around actually calculating the integral over the convolution. First we note that the Breit-Wigner propagator appears squared under the phase-space integral since we integrate over the squared matrix element. The function in the integrand approximates a Dirac distribution for small widths

$$\lim_{\Gamma \rightarrow 0} |G_{\text{BW}}(|p|)|^2 = \lim_{\Gamma \rightarrow 0} \frac{1}{(p^\mu p_\mu - m_H^2)^2 + m_H^2 \Gamma_H^2} = \frac{\pi}{\Gamma_H} \delta(p^\mu p_\mu - m_H^2) \quad (3.4)$$

There are three orders of magnitude between the Gaussian resolution and the width of the Breit-Wigner in our example. For this reason we assume that we can replace the original squared propagator by a delta distribution  $\delta(p^\mu p_\mu - m_H^2)$ . Next we carry out the integral over its four-momentum. The integral from the convolution remains and extends over the left integrand

$$G_{\text{Gauss}}(|p|) = \frac{ig_H}{\sqrt{cm_H^2 \sigma^2}} \exp\left(-\left(\frac{p^\mu p_\mu - m_H^2}{2\sigma}\right)^2\right). \quad (3.5)$$

The standard deviation  $\sigma$  is appropriately redefined to ensure that the mass dimension of the exponent is zero. Its numerical value is determined by the experimental resolution we want to implement.

Expression 3.4.2 replaces the hard coded Higgs propagator in the corresponding `Helas`-routine. The normalization constant  $c$  needs to be chosen appropriately so that the integrals over the original Breit-Wigner shape and the Gauss shape match.

Choosing a Gauss to account for the detector resolution is rather crude and only gives a minimal sense of authenticity. It is however sufficient for our example.

Figure 3.4 shows how the Gauss propagator compares to the Breit-Wigner after all cuts are applied. Our assumption to replace the Breit-Wigner propagator with a Gaussian seems well justified (notice the logarithmic scale). Additionally we show the invariant mass distribution for the Gauss propagator alone to check if it has the desired shape. The fitted normal distribution matches the form well.

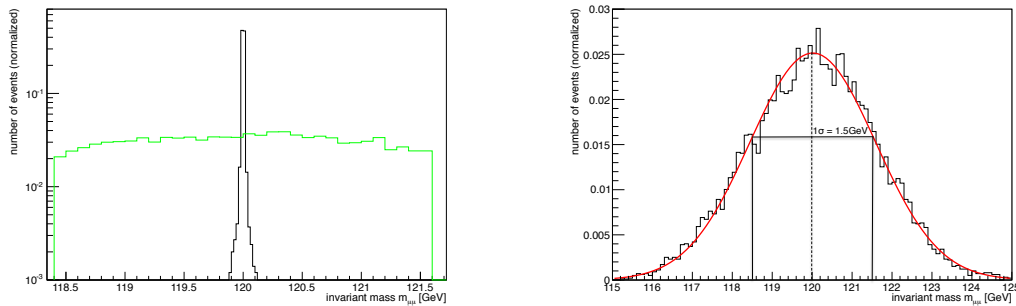


FIGURE 3.4: (left) The distribution of the invariant  $\mu^+\mu^-$  mass. Breit-Wigner propagator (black) vs the Gaussian one (green) after all cuts are applied. Both are normalized. (right) The same distribution for the Gauss without the mass cuts. A fitted normal distribution (red) matches the expectation.

### 3.4.3 Results of the Analysis

When trying to integrate the signal and background processes with `MadGraph5` one finds some of its structural weak points. These are not bugs in the code but simply limitations of the single diagram enhanced method. The signal process is the only part `MadGraph5` accurately reproduces on its own. The reasons for the issues with the other processes and how they can be resolved by our modified method are described in appendix A.2. As it turns out `MadMax` is able to produce cross sections, which are at least close to their true values, for any of the processes.

To make sure that `MadMax` integrates out and combines the processes considered we compare our results with the ones given in [7]. A summary is presented in table 3.2.

We investigate the results for three values of the Higgs mass at different center-of-mass energies. For that we picked the two values from the paper that are closest to the actual Higgs mass. Additionally we include the correct value for the Higgs mass of 126 GeV. The literature values for the background cross sections for the 126 GeV Higgs are obtained with `SHERPA` [40] and are labeled with an index <sup>1</sup>.

With these results we can conclude that `MadMax` is indeed mapping the phase spaces of all our processes sufficiently well. We continue our analysis and examine the Log-Likelihood functions calculated after the parallel integration. If these are coinciding with the ones presented in the paper as well `MadMax` met its first major benchmark.

$\sqrt{s}$	$m_H$ [GeV]	$\sigma_H^{\text{Mg}}$ [fb]	$\sigma_H^{\text{Max}}$ [fb]	$\sigma_{\text{ew}}^{\text{Lit}}$ [fb]	$\sigma_{\text{ew}}^{\text{Max}}$ [fb]	$\sigma_{\text{qcd}}^{\text{Lit}}$ [fb]	$\sigma_{\text{qcd}}^{\text{Max}}$ [fb]
14 TeV	120	0.218	0.199	0.33	0.26	2.6	1.92
	126	0.190	0.127	0.28 <sup>1</sup>	0.202	1.78 <sup>1</sup>	1.45
	130	0.165	0.152	0.24	0.19	1.61	1.23
40 TeV	120	0.591	0.522	0.694	0.532	3.32	2.361
	126	0.518	0.446	0.61 <sup>1</sup>	0.472	2.49 <sup>1</sup>	1.837
	130	0.443	0.419	0.530	0.422	2.11	1.65
200 TeV	120	3.201	2.721	4.0	3.24	29.2	23.44
	126	2.982	2.237	3.2 <sup>1</sup>	3.172	22.3 <sup>1</sup>	19.43
	130	2.234	2.044	2.7	1.97	18.7	12.91

TABLE 3.2: Cross sections for Higgs production in WBF at different energies and different Higgs masses. We compare with MadGraphs internal values just as with the ones in the paper.

MadMax combines the signal and background  $d\sigma$ 's to calculate the single-event distributions. They can be seen on the left in figure 3.5.

Next we convolve and manipulate the single-event distributions as described in section 2.3 to get to the  $n$ -event Log-Likelihood distribution. The Fourier analysis program LEPStats4LHC additionally calculates the significance of the signal over the backgrounds in terms of Gaussian standard deviations. This is done in strict correspondence with the  $CL_b$ 's we defined earlier. The only input needed are the integrated luminosity at which our search is conducted and the single-event Likelihood distributions themselves. All other parameters LEPStats4LHC can calculate on its own.

Figure 3.5 shows on the right the  $n$ -event distribution for our processes in the case of a 120GeV Higgs produced in a  $\sqrt{s} = 14\text{TeV}$  LHC collision. In this scenario one can expect a maximum significance of  $1.74\sigma$  for an integrated luminosity of  $300\text{fb}^{-1}$ .

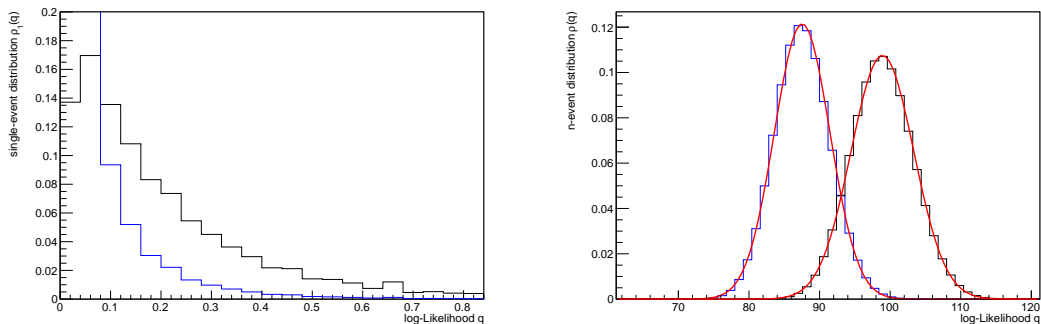


FIGURE 3.5: (left) Single-event Likelihood distributions for a 120GeV Higgs produced in WBF and decays in  $H \rightarrow \mu^+ \mu^-$  vs QCD and electroweak backgrounds. (right) the  $n$ -event distribution: we additionally fitted a Gauss curve for control (red). In both figures is the signal distribution black and the background one blue.

The distributions for the other Higgs masses and center-of-mass energies, listed in the table, are structurally equal to this one.

In a second step we let `LEPStats4LHC` do the same calculations again for different luminosities. By successively increasing the luminosities value we can find out what the least amount of luminosity is that we actually need to collect to expect a  $5\sigma$  effect. Only then discovery can be claimed.

All the results obtained from the  $n$ -event Likelihood distributions are summarized in table 3.3. We do not have reference values for the significance of a 126GeV Higgs but the values lie well within the expected range.

$\sqrt{s}$	$m_H$ [GeV]	significance $\sigma^{\text{Lit}}$	significance $\sigma^{\text{Max}}$	$\mathcal{L}_{5\sigma}^{\text{Lit}}$ [ $\text{fb}^{-1}$ ]	$\mathcal{L}_{5\sigma}^{\text{Max}}$ [ $\text{fb}^{-1}$ ]
14 TeV	120	1.8	1.74	2300	2450
	126	-	1.71	-	2600
	130	1.7	1.66	2700	2750
40 TeV	120	3.3	3.12	700	770
	126	-	3.14	-	800
	130	3.2	2.97	750	810
200 TeV	120	5.7	5.49	230	260
	126	-	5.03	-	300
	130	5.3	4.92	260	320

TABLE 3.3: The significances of the signal over the irreducible backgrounds for WBF Higgs production and subsequent decay  $H \rightarrow \mu^+ \mu^-$  at a Luminosity of  $300\text{fb}^{-1}$ . As a first benchmark we cross check with the numbers presented in the original paper. Additionally we compare the luminosity  $\mathcal{L}_{5\sigma}$  for which a  $5\sigma$  significance is found.

The results obtained with `MadMax` are in good agreement with the ones presented in [7]. The discrepancies which appear are order of magnitude 10% effects.

The remaining differences are partially due to the fact that we use a different version of `MadGraph` than the original paper did. As we stressed in the last section the best possible integration would need to optimize on the entire integrand consisting of a logarithm of a ratio of cross sections. Since the logarithm is a monotonous function it would already be sufficient to optimize on the ratio of the  $d\sigma$ s. The numbers presented in table 3.3 show that `MadMax` is performing already well with our modified single diagram enhanced method - at least for the processes we consider.

Having verified the results of an earlier analysis `MadMax` has met an important benchmark point. We are feeling confident to perform an analysis of a real-life processes found at the LHC. The next chapter examines Higgs-Strahlung as the production channel for the Higgs and a subsequent decay to a  $b\bar{b}$  pair.

## Chapter 4

# Higgs-Strahlung and decay to $b\bar{b}$ - Beyond Thunderdome

### 4.1 Setting up the Process

We complete the introduction of MadMax by investigating one last realistic process. For this we chose a Higgs produced by Higgs Strahlung, i.e. a Higgs that is radiated off of a Z boson. The production is then followed by a subsequent decay to a  $b\bar{b}$  quark pair. The Z we do not let decay in the final state. Higgs-Strahlung was first proposed as a Higgs production channel in [41].

The reason one would want to examine this process is simple. The production mechanism again probes the  $VVH$ -coupling described in 2.13 just as the WBF production does. Higgs-Strahlung is additionally one of the cleanest production channels available. It is buried under backgrounds which are order of magnitude bigger than the signal. Those background are however mostly structureless and allow for a good identification of the signal.

The decay to the  $b\bar{b}$  pair gives us inside on the structure of the quark-Yukawa-coupling described in 2.18. We chose to look at the  $b\bar{b}$  pair for this since the branching ratio  $\text{BR}(h \rightarrow b\bar{b})$  is dominating the decay for a SM-Higgs of mass 126GeV.

The mentioned irreducible backgrounds are again a purely electroweak and a partially QCD one with final state Z radiation. Exemplary Feynman diagrams for the processes can be seen in figure 4.1.

Since Tevatron was a proton antiproton collider Higgs-Strahlung was supposed to be the dominating production channel in a Tevatron Higgs search. More insight on the process can be gained from [42]. The summary of the experimental results of this search can be found in [43].

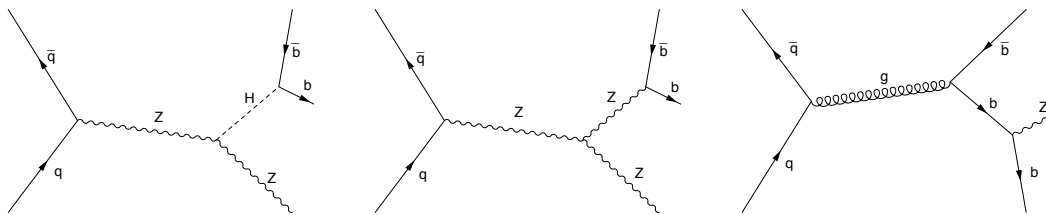


FIGURE 4.1: Representative Feynman diagrams for the signal and the backgrounds. We have Higgs production via Higgs Strahlung (left), the purely electroweak background (middle) and the QCD background (right).

At the LHC on the other hand Higgs-Strahlung is heavily suppressed. It cannot be a dominating channel since it requires an initial state antiquark. In a proton proton collision this can not be

realized. It was however shown for our exact process (including the decay to b-quarks) in [44] that the channel contributes considerably to the total production cross sections at high transverse momenta  $p_T$  once the right jet reconstruction is employed.

The external parameter input follows closely the one found for WBF. Again we investigate a 120GeV Higgs produced at a 14TeV LHC. Overall we use the same acceptance cuts as in the previous example but chose our Higgs mass-window to be between 108GeV and 132GeV for the  $b\bar{b}$  pair. These values are limited mostly through the detector resolution.

The detector effects themselves are again modeled by smearing the Breit-Wigner shape of the Higgs propagator with a Gaussian just as we did in the WBF example. The standard deviation is set by the experimental resolution which we take to be 12GeV. Figure 4.2 shows the invariant mass distribution of the  $b\bar{b}$  which follows the described Gaussian.

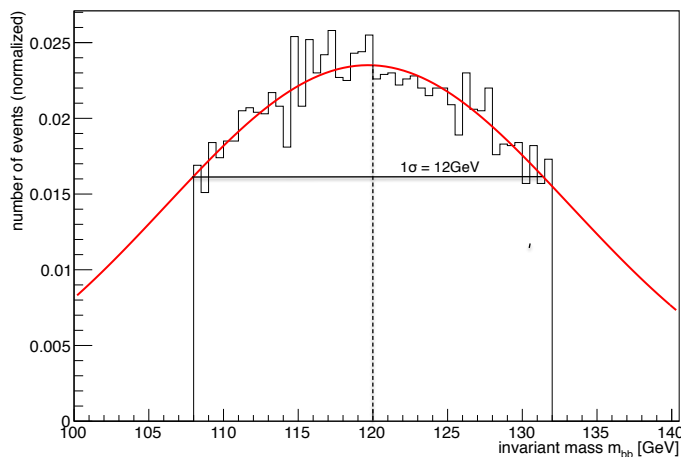


FIGURE 4.2: The distribution of the invariant mass of the  $b\bar{b}$  pairs coming from a 120GeV Higgs produced in Higgs-Strahlung at  $\sqrt{s} = 14\text{TeV}$ .

## 4.2 Results of the Analysis

Since we do not have literature values for reference our only back-up check is to produce all the processes with **MadGraph** once and compare the cross sections calculated by **MadMax**. Even though the backgrounds have different pole structures we see that already for a sensible event sample we are accurate enough to continue. See table 4.1 for the results of the integrations.

	$\sigma_{\text{ZH}}[\text{pb}]$	$\sigma_{\text{ew}}[\text{pb}]$	$\sigma_{\text{QCD}}[\text{pb}]$
<b>MadGraph5</b>	0.502	0.05	15.97
<b>MadMax</b>	0.50	0.05	13.46

TABLE 4.1: Comparison of the cross sections produced by **MadGraph5** and **MadMax** for a Higgs radiated of a Z and successively decays into a  $b\bar{b}$  pair. The external parameters are described in the text.

The combined optimization procedure accurately maps the phase space precisely enough. Since we are only dealing with few intermediate particles the pole structure of our processes is fairly simple. For this reason are the cross sections additionally matching the values produced by

## MadGraph5.

For a realistic analysis we cannot keep the the final state  $Z$  stable. We will compensate for the missing decay (and further aspects not considered yet) by introducing  $k$ -factors to the cross section. The  $k$ -factors employed in our analysis are described and calculated in [46]. We limit ourselves to listing them here. The cross sections presented in 4.1 already include these  $k$ -factors.

First of all we do not account for the decay of the  $Z$  in the final state. The leptonic branching ratio  $\text{BR}(Z \rightarrow \text{lep})$  we take to be 0.067. This becomes an additional multiplicative factor to the cross section.

Secondly there is only a finite tagging-efficiency on the b-quarks. For our scenario we found it to be 0.6 per quark which means a total  $k_{\text{tag}}$ -factor of  $(0.6)^2 = 0.36$  for the tagging-efficiency. Due to mistaggs the cross section decreases.

Thirdly is our matrix element only calculated at tree level. If we wish to account for next-to-leading order effects this can be done using  $k_{\text{NLO}} = 1.3$ . The radiative corrections increase the cross section. Lastly we must stress that we excluded final state jets from our analysis. These are however a vital part of the QCD background. They can be included by merging our sample with the corresponding background sample containing jets ( $\sigma_{\text{jet}} = 35.4\text{pb}$ ). The  $k$ -factor is given in our reference as 2.5.

Multiplying all the factors we end up with  $k_{\text{sig}} = 0.031356$  for the signal,  $k_{\text{ew}} = 0.02412$  for the electroweak background and  $k_{\text{QCD}} = 0.0603$  for the QCD background. We additionally account for background uncertainties by giving 20% error bars on these values.

The next step is of course to find the Log-Likelihood distribution functions. In [45] the results of the analysis are presented.

In strict analogy to our WBF-example we first produce the single-event and convolve them to find the  $n$ -event distributions. Figure 4.3 displays the results.

When employing LEPStat4LHC we immediately receive the maximal expected significance for the signal over the backgrounds. For an integrated luminosity of  $100\text{fb}^{-1}$  it turns out to be  $1.8\sigma$ . Iteratively we find that we would need at least to collect an integrated luminosity of  $2900\text{fb}^{-1}$  to produce a  $5\sigma$  effect.

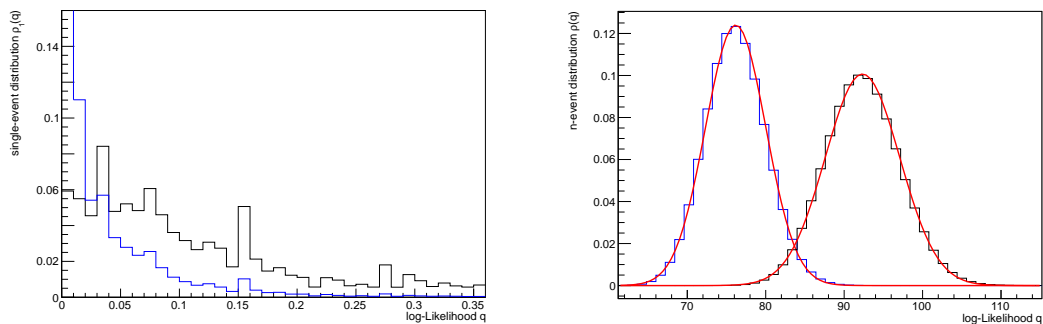


FIGURE 4.3: (left) Single-event Likelihood distribution for Higgs-Strahlung with subsequent decay to a  $b\bar{b}$  pair over as compared to its backgrounds.

(right)  $n$ -event Likelihood distribution calculated from the single-event distributions.

The signal distribution is in both figures black while the background is blue. The Gaussian fit in the right figure is in red.

Calculating the maximum expected significance is only the first step of our analysis. We still want to find out where in phase space the significance is actually collected. This is exactly the situation MadMax was built for.

Figure 4.4 shows the distributions of the invariant mass  $m_{b\bar{b}}$  for the  $b\bar{b}$  pair for the signal and backgrounds. On the right hand side it presents the corresponding distributions for the



transverse momentum  $p_T$  of the reconstructed particle. We also included the uncertainty curves coming from the 20% error bar of the overall  $k$ -factor.

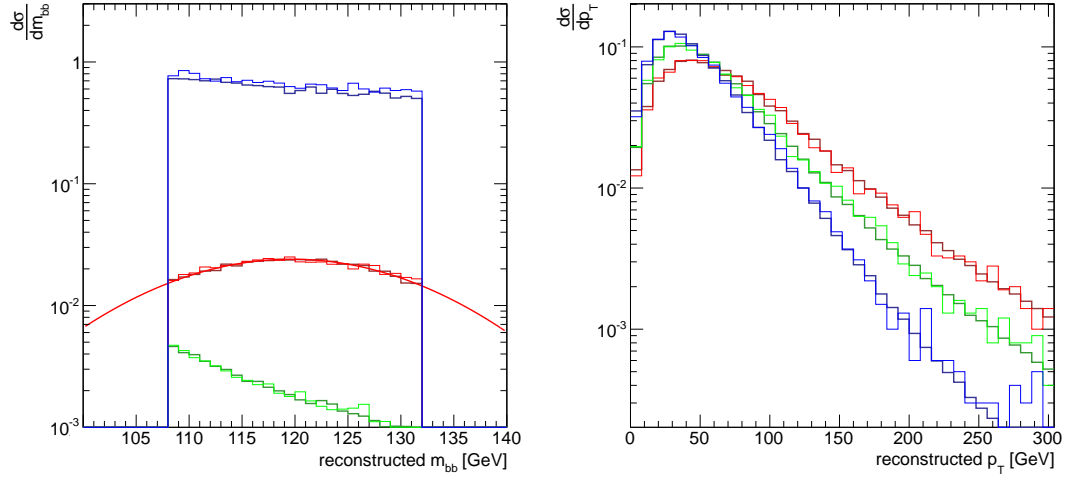


FIGURE 4.4: Kinematic distributions of the  $b\bar{b}$  pair. The signal distributions ( $H \rightarrow b\bar{b}$ ) are in red, the electroweak backgrounds in green and the QCD process in blue.  
 (left) The distribution of invariant mass - notice the Gaussian shape of the signal.  
 (right) The transverse momentum of the reconstructed  $b\bar{b}$  pair.

We will now integrate the same process over different regions in phase space. This can be achieved by enforcing different kinematic cuts for each run. With this strategy we can find out where the biggest contributions to the significance come from. We simply check the significance after each integration until it starts dropping considerably. This procedure can, in general, be employed to any kinematic variable or even a mixture of different ones.

As an example we increase the cut on the transverse momentum  $p_T$  of the Higgs reconstructed from the  $b\bar{b}$  pair. This is done in slices of 50 GeV which should give us an idea in which  $p_T$  region the significance is collected. The resulting distribution is shown in 4.5. We included 20% error bar on the  $k$ -factors just as we did before. The additional paler lines show the corresponding uncertainty in significance.

Distributions like the one we present here might give us a hint where in phase space the significance is actually collected. This knowledge is immensely useful because it can give us insights on how to optimize e.g. a search for the Higgs and his properties. It enables us to identify the signal-rich regions of phase space which in turn helps us to know what aspects of the search need to be carried out especially careful.

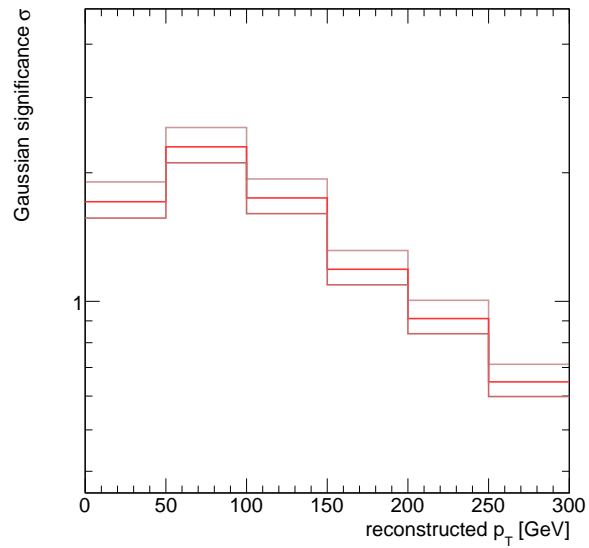


FIGURE 4.5: We successively increase the  $p_T$  cut by 50GeV to find out in which phase space region the significance is collected. The significance found for each sample is shown on the y-axis.

We can draw immediate conclusions from the analysis of the Higgs's  $p_T$  presented. The largest contributor to the significance of our process are Higgs bosons with a transverse momentum  $p_T$  between 50GeV and 100GeV. All other  $p_T$  slices are delivering significances considerably smaller than the one found in this region (notice the logarithmic scale!).

When trying to measure the coupling to the  $b\bar{b}$  pair it is therefore absolutely fundamental to accurately reconstruct the Higgs from the quarks in this particular region. The most important way of realizing this would be to construct a b-tagger that has optimal tagging efficiency when dealing with  $p_T$ 's between 50GeV and 100GeV.

## Chapter 5

# Conclusions and Outlook

In this thesis we presented the tool **MadMax** and the fundamental concepts underlying its construction. Making use of the multi-purpose event generator **MadGraph5** we have now a possibility to automatically calculate the maximum expected significance for a given signal process over its backgrounds.

It was shown that it can accurately reproduce the results of earlier Likelihood analysis for an LHC Higgs search. The results for a Higgs produced in weak boson fusion that subsequently decays into a  $\mu^+\mu^-$  pair have been confirmed by **MadMax**.

Additionally we applied our method to a process that has not yet been inspected with the help of a Likelihood analysis. We investigated a Higgs produced in Higgs-Strahlung which probes the same gauge couplings weak boson fusion does. The production was followed by a decay of the Higgs to a  $b\bar{b}$  pair. Our analysis showed that most of the significance is actually collected for the  $p_T$  of the Higgs lying between 50GeV and 100GeV.

The processes we considered are not playing a dominant role in the discovery of the Higgs at the LHC. Its discovery is on the other hand only the first step in validating the role it plays in the Standard Model. The only way to make sure that the mechanism of electroweak symmetry breaking is realized in nature in the way it is described in the model is to examine all the couplings predicted by it.

Especially the processes involving the couplings to the lighter matter generations suffer from low signal rates that are hard to distinguish from background. This is precisely why we chose to further investigate them. They are an ideal playground to take **MadMax** to the test and learn about its strengths and weaknesses. The low signal rates and the more or less shapeless background event distributions e.g. in the weak boson fusion process are well suited to be examined by our tool and show its predictive power.

The major issue with **MadMax** is that one needs to decide what it should be used for. It can perfectly well be used as an integrator. This is however only possible if one optimizes on the signal process only. The corresponding background processes calculated in the parallel integration are, in general, completely wrong. Since the four-momenta are optimized for the signal process they have no chance of mapping the pole structure of the background correctly as well.

Parallel integration is on the other hand not the application for which **MadMax** was built. The goal is to calculate the Log-Likelihood distribution for signal and irreducible backgrounds. For this endeavor it is crucial that we do accurately map the poles of signal and background simultaneously. In the end it is the poles that determine where in phase space the Likelihood function takes large values and where we need to integrate very carefully.

We resolved this issue by introducing a combined signal and background optimization. The price one pays to map the Log-Likelihood is that the resulting four-momenta are not fit to integrate the cross sections as well. In the end one has to choose between an accurate cross section or the correct significance analysis. Both at the same time are with the methods presented not possible.

The version of **MadMax** we presented in this thesis is only a first step to create a powerful tool for the calculation of the maximum expected significance. It still has great potential for improvement.

We have been using a rather crude way of mimicking the finite detector resolution. Changing to a more rigorous way of simulating the detector effects will have a great impact on the analysis. One way could involve the so-called Cousins-Highland method presented in [47]. An application to LHC physics and our special needs can be found in [48].

Continuing along these lines we must stress again that we are using a parton level event generator. We have not even begun to capture all the physics happening before and after the hard process took place. Not everything that can happen will influence the outcome for the significance but including physics beyond the hard process is something we definitely need to look into in the future.

Even on the parton level there is still work to be done. We only tested **MadMax** for Standard Model processes. We will still need to test it extensively for theories going beyond the Standard Model. This might present us with interesting insights for the search for new physics. Some of these models are already implemented in **MadGraph5** and **MadMax** only needs to be customized to them. These are some of the aspects we will focus on in the future.

So in the end we did manage to answer some of the questions posted in the beginning. By having laid the fundament we have made at least a step towards the solution. We are now in a position that is fairly close to what we were looking for. Being able to see where in phase space the significance is collected is not only handy when trying to confirm predictions made by established theories or improve on results we already are familiar with. It also allows us to predict where to look for new physics for which there has no experimental support been found yet.

## Acknowledgements

My first thanks go to Tilman Plehn for offering me the opportunity to begin and work on the MadMax project while also providing me with help and guidance - not only for the project but also throughout my emigration.

The reasons to thank my collaborator and friend Peter Schichtel would fill an appendix on their own so I am simply going to say 'man - I owe you big time!'.

I am just as thankful for working with the entire Heidelberg Pheno Crew who did their best to keep me sane during the insane times this year. A special 'thank you' goes to Torben Schell for his never ending tech support.

I also would like to thank Kyle Cranmer for explaining the Fourier tool LEPStats4LHC to us, Johan Alwall for the helpful discussions concerning MadGraph5 and Jan Pawlowski for agreeing last minute to be my co-referee.

Additionally I am in debt to the Pittsburgh Department of Physics and especially to Ayres Freitas and Richard Ruiz for supporting me during my end game and keeping their patience with me.

Last but not least to my parents, friends and family - for always having my back.



# Appendix A

## Set-Up of the WBF Processes in MadGraph5

If one naively tries to reproduce the signal process and the two backgrounds described in the original paper [7] using MadGraph5, the results obtained turn out to be various orders of magnitude too small. The problems are various issues with the input parameters of the model, the cuts implemented and weak-points in MadGraph5s integration algorithm. This appendix describes the ways to fix the underlying bugs in and technical difficulties appearing.

### A.1 Signal-Process

#### A.1.1 Correcting the Higgs Width

The first major source of error appears when trying to set up the signal process  $p p \rightarrow h j j$  QED = 3 QCD = 0,  $h \rightarrow \mu^+ \mu^-$  QED = 1 QCD = 0. The problem when trying to reproduce the results is the fact that they were obtained using another Higgs decay-width than the one automatically used by MadGraph5. This becomes evident, if one checks the branching ratio of the Higgs to muons.

MadGraph5 gives for the process  $h \rightarrow \mu^+ \mu^-$  QED=1 a decay width of

$$\Gamma_{\mu\mu} = (8.79 \pm 0.019) \times 10^{-7} \text{GeV}. \quad (\text{A.1})$$

For comparison one finds the full decay width of the Higgs (coming from all decay products) which is implemented hard in *parameter\_card.dat* to be

$$\Gamma_{\text{full}} = 5.75 \times 10^{-3} \text{GeV} \quad (\text{A.2})$$

These numbers we can combine to give branching ratio for the Higgs to Muon decay  $H \rightarrow \mu^+ \mu^-$  of roughly

$$BR(h \rightarrow \mu\mu) = \frac{\Gamma_{\mu\mu}}{\Gamma_{\text{full}}} = 0.15. \quad (\text{A.3})$$

That this result needs to be fixed becomes evident if one considers the original branching ratio assumed in the paper. This was assumed to be  $0.24 \times 10^{-3}$ , which is off by 40% to the number used in `MadGraph5`.

To fix this issue and reproduce the true cross section from the paper we use `hdecay` [49]. With this piece of software we can calculate the branching ratios and total decay width for a SM Higgs boson for all the Higgs masses we are interested in. The so found decay widths we then hard-code into `MadGraph5` for each mass we are considering.

`hdecay` delivers for such a SM-Higgs with a mass of 120GeV a branching ratio for the decay to  $\mu^+\mu^-$  of

$$BR(h \rightarrow \mu\mu) = 0.2439 \times 10^{-3}. \quad (\text{A.4})$$

Since we know what  $\mu^+\mu^-$  branching ratio we want `MadGraph5` to use in the end we can calculate back to the full decay width so we match the numbers in the paper precisely.

$$\Gamma_{\text{full}} = \frac{\Gamma_{\mu\mu}}{BR(h \rightarrow \mu\mu)} = 3.604 \times 10^{-3} \text{GeV}, \quad (\text{A.5})$$

instead of taking `hdecay` total decay width which is off from that value by a few percent. With that new width the resulting cross section is a lot closer to original cross section of  $\sigma = 0.22\text{fb}$ . For different masses used in the analysis we found the corresponding `hdecay` widths and the corrected ones along the same lines to be

$m_H$	115GeV	120GeV	126GeV	130GeV	140GeV
$\Gamma_H[10^{-3}\text{GeV}]$	3.124	3.512	4.221	4.920	8.196
$\Gamma_H^{\text{corr}}[10^{-3}\text{GeV}]$	3.205	3.604	4.332	5.049	8.411

TABLE A.1: Higgs width for different masses calculated with `hdecay` - the second row gives the values corrected to coincide with the ones used in [7]

### A.1.2 The CKM Matrix

In order to save calculation time we switch off quark-mixing described through the CKM-matrix. Therefore it is not sufficient to use the already implemented model *sm-ckm*, since this reduced standard model does not contain the Yukawa-coupling of the Higgs like `MadGraph5`'s small Standard Model *sm*. Instead we import the full standard model *sm-full* and simply switch the CKM-matrix to a diagonal form by setting the Wolfenstein-parameter  $\lambda$  to 0.

### A.1.3 Implementable Cuts

After fixing the external parameters we proceed and implement the cuts. The first group are the acceptance cuts on the  $\mu^+\mu^-$  pair and the jets. For the jets this means that we only accept events with

$$p_{T_j} \geq 20\text{GeV} \text{ and } |\eta_j| \leq 4.5 \quad \text{and} \quad \Delta R_{jj} \geq 0.6 \quad (\text{A.6})$$



while the acceptance cuts on the  $\mu^+\mu^-$  pair are analogously given to be

$$p_{T_\mu} > 10\text{GeV with one having at least } p_{T_\mu} > 20\text{GeV} \quad (\text{A.7})$$

on the transverse momenta of the pair. Additionally we cut

$$|\eta_\mu| < 2.3 \text{ and } \Delta\eta_{\mu j} > 0.6 \quad (\text{A.8})$$

on their pseudo-rapidity.

Two Notes on the geometric cuts: the separation cut on the jets is customarily defined as  $\Delta R_{jj} = \sqrt{\Delta\phi_{jj}^2 + \Delta\eta_{jj}^2}$ . The difference in pseudo-rapidity of a single  $\mu$  and one of the jets is not an eligible option in **MadGraph5**. Therefore it has to be hard-coded into *cuts.f*. This however is straight forward by simply mimicking the other difference cuts already present.

Furthermore we will require the reconstructed invariant jet mass to be  $m_{jj} \geq 500\text{GeV}$  for LHC and larger than  $1000\text{GeV}$  at a very Large Hadron Collider (vLHC) with center of mass energy of  $40\text{GeV}$  and  $200\text{GeV}$  respectively. Accordingly we require the reconstructed invariant mass of the  $\mu^+\mu^-$  pair to be in the mass-window around the Higgs mass:  $118.4\text{GeV} < m_{\mu\mu} < 121.6\text{GeV}$ , when cutting on the events.

Finally to account for the detector geometry we apply the weak-boson-fusion cuts

$$|\eta_{j_1} - \eta_{j_2}| \geq 4.2 \quad \eta_{j_1} \times \eta_{j_2} < 0. \quad (\text{A.9})$$

With those cuts implemented one is able to reproduce the cross sections found in the paper up to 10% culcancy.

## A.2 Background-Processes

Next we are trying to reproduce the two irreducible background processes. If one sets up the electroweak and QCD process in **MadGraph5** one runs however into problems not fixable in **MadGraph5**. We describe why this happens and why it does not matter for **MadMax** which is perfectly capable of integrating them all correctly.

### A.2.1 Electroweak Background

The first background is purely electroweak:  $p p \rightarrow j j \mu^+\mu^- /h$  QED=4 QCD=0. We apply all of above cuts. A successive application shows no deviation (up to 10% culcancy) in cross section from a simulation conducted with SHERPA [40], until the last mass-window cut is applied.

Table A.2 summarizes the double comparison we did to be on the save side. The first line are the cross sections procuded by **Sherpa** using its internal cut. The form cutting an uncut **Sherpa** sample manually are listed next. The manual cutting is done using ROOT [50].

We do the same for **MadGraph5** and an uncut sample produced by it. In the end we list the deviations between the internally and externally cut samples from both generators. It becomes clear that the mass window cut is the main source of error. Up until that last cut is applied we are only facing a 10% deviation which is a discrepancy between event generators and thus

expected.

cuts	Sherpa[fb]			MadGraph5[fb]			relative	
	internal	external	dev.	internal	external	dev.	internal	external
uncut	1495	1495	0%	1403	1403	0%	6.2%	6.2%
$m_{jj} > 500\text{GeV}$	89	88	0.8%	79	78	0.3%	11.7%	11.2%
$118.6\text{GeV} < m_{\mu\mu}$ $121.6\text{GeV} > m_{\mu\mu}$	0.34	0.32	5.9%	0.012	0.25	95%	96%	23.5%

TABLE A.2: cutflow-comparison **MadGraph5** vs **Sherpa** - as well as the comparison of the cuts with externally applied ones.  $m_{jj} > 0$  means all cuts up until and including  $m_{jj}$  are applied.

If one has a look into the distributions of the kinematic variables after all cuts are applied the reason for the deviating cross section becomes evident. Figure A.1 shows the distributions of the jets rapidities. Since the system enjoys rotational invariance around the beam axis there should be not preferred hemisphere for the jets, i.e. the distributions should be symmetrical (**Sherpa** - green). We however see a preferred hemisphere for the jets of **MadGraph5** (black).

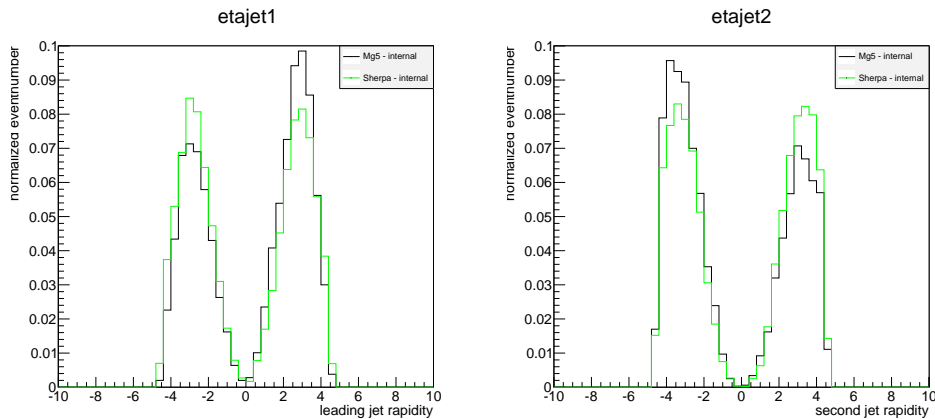


FIGURE A.1: The rapidity distribution of the leading jet (left) and the second jet (right). We see a clear asymmetry in both, i.e. both have a preferred hemisphere.

The problem is a **MadGraph5** inherent flaw. Part of it can be fixed by allowing the Z in the s-channel diagrams to go off-shell which was previously not possible. This takes care of the misaligned jets. Figure A.2 shows the distributions after a patch fixes the Z off-shell issue. Both jets are now perfectly isotropically reflected in the now symmetric distributions.

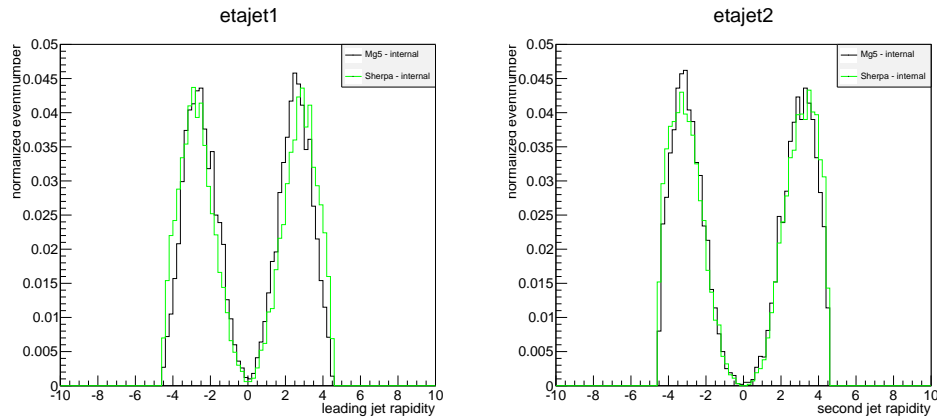


FIGURE A.2: The rapidity distribution of the leading jet (left) and the second jet (right). No hemisphere is preferred the - the jets are isotropically distributed around the beam axis.

The cross sections are however unaffected by this. The the single diagram enhanced technique which it employs to integrate the phase space of the processes is not capable of integrating the backgrounds correctly. Apparently the pole structure of the matrix element under consideration does not agree well with the restrictive cuts applied. In the narrow window around the Higgs mass hardly any events are found by **MadEvent**. While we are looking in a neighborhood close to the Higgs mass the pole sits on the Z peak. This means that the integrator does not have a chance to find any events since it optimizes on the pole structure of the Z.

The problem can not be fixed any further. The value of the cross section improves however significantly once we let **MadMax** parallel integrate. The reason being that **MadMax** uses the four-momenta optimized around the Higgs pole in the signal process for the background as well. Regardless of the phase space limitations are both structures correctly mapped by **MadMax**.

## A.2.2 QCD Background

The second irreducible background is the QCD process. When trying to run  $p p > \mu^+ \mu^- / h$  QED=2 QCD=2 we encounter the same problems as for the electroweak background. The cross sections after the patch fixing the on-shell Z are still orders of magnitude too small.

Once again the cut on the muons mass is too restrictive for **MadGraph5s** integration technique. Here we are even farther away from the 120GeV region of the mass window cut. The pole structure of the diagrams are now suffering from a gluon-pole, which goes like inverse center of mass energy squared. Far out around the Higgs pole hardly any events are found by **MadGraph5**. The phase space again is not mapped correctly.

We see however an improvement for the QCD cross sections as well as soon as we use signal optimized four-momenta when integrating with **MadMax**.

## Appendix B

# Comparison of the MadGraph5 and the MadMax-Integration

To proof that `MadMax` does actually calculate its processes correctly this appendix contains a detailed list of all processes and their respective cross sections generated by `MadGraph5` and `MadMax`.

This also serves the purpose of giving an overview over how much the cross sections deviate from the original ones, once we use four-momenta that are optimized on a signal process with a pole structure different from the one under consideration.

### B.1 Purely Leptonic Processes

We start with purely leptonic processes. Here we do not need to care about the tricky implementation of the parton distribution functions, factorization scales and all these technicalities. This section serves to proof that the matrix elements themselves are called and processes right. It becomes immediately apparent, that for purely electroweak processes we do not need much statistics - the cross sections already coincide extremely well. Table [B.1](#) stars us off with one the simplest processes calculateable with `MadGraph5` consisting only of two diagrams.

	signal $e^+e^- \rightarrow e^+e^-$ QED = 2	background 1 $e^+e^- \rightarrow \mu^+\mu^-$ QED = 2	background 2 $e^+e^- \rightarrow \tau^+\tau^-$ QED = 2
<code>MadGraph5</code>	$0.2203 \pm 0.02$ pb	$(5.3 \pm 0.2) \times 10^{-4}$ pb	$(5.3 \pm 0.2) \times 10^{-4}$ pb
<code>MadMax</code>	$0.2181 \pm 0.2$ pb	$(5.4 \pm 0.6) \times 10^{-4}$ pb	$(5.4 \pm 0.6) \times 10^{-4}$ pb

TABLE B.1: Simple 2-2 purely leptonic scatterings; due to the same pole-structure no major deviations occur for 1000 events.

In all processes under consideration the default settings of `MadGrappg5` were used if not specifically mentioned differently. That especially means we are running in LHC mode. That is done in

`MadGraph5` with two beams of protons with 7TeV. The events are generated using the templates `run_card.dat` (fixing the cuts) and `parameter_card.dat` (fixing the model parameters).

But even if we change the pole-structure to slightly more realistic analysis the supplied statistics is already enough to ensure stable results. Table B.2 compares the Breit-Wigner pole structure of an intermediate Higgs or Z with the  $1/s$  structure of a photon.

	signal $e^+e^- > h > \mu^+\mu^-$	background 1 $e^+e^- > a > \mu^+\mu^-$	background 2 $e^+e^- > Z > \mu^+\mu^-$
<code>MadGraph5</code>	$0.2203 \pm 0.02$ pb	$(5.3 \pm 0.2) \times 10^{-4}$ pb	$(5.3 \pm 0.2) \times 10^{-4}$ pb
<code>MadMax</code>	$0.2181 \pm 0.2$ pb	$(5.4 \pm 0.6) \times 10^{-4}$ pb	$(5.4 \pm 0.6) \times 10^{-4}$ pb

TABLE B.2: Higgs search at an electron-positron collider - all cross sections are well recovered for 1000 events.

The third case of interest here contains final or initial state radiation. Due to its soft divergences through the final state photons `MadGraph5` has generic problems integrating the matrix element over the full phase space. To take care of the pole structure of the final state photons we will cut on the  $p_T$  of the photons just as well their distance  $R_{aa}$ . This ensures convergence in the `MadGraph5` integration. Various final state photons are calculated in B.3

	signal 1 $e^+e^- > \mu^+\mu^-a$	signal 2 $e^+e^- > \mu^+\mu^-aa$	signal 3 $e^+e^- > \mu^+\mu^-aaa$
<code>MadGraph5</code>	$0.2203 \pm 0.02$ pb	$(5.3 \pm 0.2) \times 10^{-4}$ pb	$(5.3 \pm 0.2) \times 10^{-4}$ pb
<code>MadMax</code>	$0.2181 \pm 0.2$ pb	$(5.4 \pm 0.6) \times 10^{-4}$ pb	$(5.4 \pm 0.6) \times 10^{-4}$ pb

TABLE B.3: Final state radiation. We list the signal process only since we only want to see how `MadMax` deals with the soft divergencies - 1000 events.

This concludes our discussion of leptonic processes. We now move ahead to QCD processes.

## B.2 Semi-Leptonic Processes

After `MadMax` apparently is calling the matrix elements and symmetry factors the way its expected to we can turn to all other factors playing a role for the final integral. The big question is if the pdfs are working correctly and the structure of the strong couplings are set in the right way. The numerical values of the couplings are fixed since all scales have been set to fixed values. This becomes necessary when one realizes that for a signal and background optimization consisting of many different processes a scale can not be defined anymore in a physically meaningful way. The coupling however comes with a complex structure calculated by `MadGraph5` every time. It remains to be determined if we call them correctly.

We run `MadGraph5` in LHC-mode, with again the default cuts and parameters.

Looking at leptonic final states the simplest processes imaginable are again consisting only of few diagrams. First results are summarized in [B.2](#)

No. events	signal	background 1	background 2
	$pp > e + e - / a$	$pp > \mu + \mu -$	$pp > e + e - / z$
MadGraph5	$717.2 \pm 1.5$ pb	$949.6 \pm 1.7$ pb	$234.1 \pm 0.8$ pb
1000	$715.0 \pm 10$ pb	$966.6 \pm 60$ pb	$263.5 \pm 80$ pb
10000	$720.4 \pm 5$ pb	$964.0 \pm 15$ pb	$244.9 \pm 20$ pb
100000	$716.9 \pm 0.1$ pb	$962.4 \pm 6$ pb	$249.1 \pm 1$ pb

TABLE B.4: Proton collisions producing lepton pairs for **MadMax** with different statistics.

The numbers suggest that **MadMax** works perfectly fine. This leads us to the assumption that the pdfs are correctly implemented. Additionally it seems that we calculate the structure of the couplings correctly.

There is one other case of interest left in the scenario of hadronic initial states and leptonic final ones. It is again the occurrence of massless final state particles which can not only be photons but gluons as well now that the QCD couplings are implemented. [Table B.5](#) shows the results for final state gluons. By increasing their number we succesively test if the quark-gluon coupling, the three-point and the four-point gluon coupling are correctly working.

	signal 1	signal 2	signal 3
	$pp > \mu^+ \mu^- g$	$pp > \mu^+ \mu^- gg$	$pp > \mu^+ \mu^- ggg$
MadGraph5	$0.2203 \pm 0.02$ pb	$(5.3 \pm 0.2) \times 10^{-4}$ pb	$(5.3 \pm 0.2) \times 10^{-4}$ pb
MadMax	$0.2181 \pm 0.2$ pb	$(5.4 \pm 0.6) \times 10^{-4}$ pb	$(5.4 \pm 0.6) \times 10^{-4}$ pb

TABLE B.5: Initial state radiation. We list the signal process only since we only want to see how **MadMax** deals with a single gluon coupling - 1000 events.

The results seem to be comparable to the photon case. We have however more gluon vertices present than in the photon case due to the self-interaction. The cross sections additionally coincide point-wise. This suggests that the correct coupling structure is called for each vertex.

### B.3 Purely Hadronic Processes

Finally we can turn to the at LHC dominating QCD-processes.

We start a simple two to two proces. The production of two jets in a LHC proton-collision comes with a lot of different subprocesses which we need to combine correctly. Additionally we can have a look if all channels are correctly mapped. [Figure B.6](#) summarizes the results.

Subprocess	MadGraph5	MadMax
P0_gg-gg	$5.32 \times 10^8 \text{pb}$	$5.41 \times 10^8 \text{pb}$
P0_gg-qq	$1.39 \times 10^7 \text{pb}$	$1.41 \times 10^7 \text{pb}$
P0_qg-qq	$1.29 \times 10^8 \text{pb}$	$1.26 \times 10^8 \text{pb}$
P0_qg-gq	$1.29 \times 10^8 \text{pb}$	$1.34 \times 10^8 \text{pb}$
P0_gq-qq	$1.29 \times 10^8 \text{pb}$	$1.37 \times 10^8 \text{pb}$
P0_gq-gq	$1.29 \times 10^8 \text{pb}$	$1.28 \times 10^8 \text{pb}$
P0_qq-gg	$3.28 \times 10^5 \text{pb}$	$3.30 \times 10^5 \text{pb}$
P0_qq-qq	$2.31 \times 10^7 \text{pb}$	$2.28 \times 10^7 \text{pb}$
total cross section	$8.25 \times 10^8 \text{pb}$	$9.16 \times 10^8 \text{pb}$

TABLE B.6: The partial cross sections for the QCD dijet production

Notice that these are simply all final and initial state combinations of quarks and gluons since we restrict ourselves to pure QCD processes. All these channels seem to get properly mapped and in the end correctly combined.

Now we run the same process with an electroweak background and optimize on each on successively - first with reduced then full proton content. Figure B.7 shows the results.

	QCD - sig	QED - bkg	QCD - bkg	QED - sig
Mg5 reduced	$7.88 \times 10^8 \text{pb}$	$6.55 \times 10^4 \text{pb}$	$7.88 \times 10^8 \text{pb}$	$6.55 \times 10^4 \text{pb}$
MadMax reduced	$8.14 \times 10^8 \text{pb}$	$4.42 \times 10^5 \text{pb}$	$7.17 \times 10^8 \text{pb}$	$5.82 \times 10^5 \text{pb}$
Mg5 full	$8.26 \times 10^8 \text{pb}$	$1.33 \times 10^5 \text{pb}$	$8.26 \times 10^8 \text{pb}$	$1.33 \times 10^5 \text{pb}$
MadMax full	$9.16 \times 10^8 \text{pb}$	$0.89 \times 10^5 \text{pb}$	$7.31 \times 10^8 \text{pb}$	$1.16 \times 10^5 \text{pb}$

TABLE B.7:  $pp > jj$  once optimized on signal and once on the electroweak background - and with full and reduced (light quarks) proton content.

Next we have a look how increased statistics in influencing the outcome in a simple two to two scattering process. Again we chose for the signal pole structure the Breit-Wigner of the Higgs.

The backgrounds consist of the already known QCD pole and a mixed electroweak process. Figure B.8 shows the results.

No. events	signal $pp > h > jj$	background 1 $pp > za > jj$	background 2 $pp > g > jj$
MadGraph5	$0.0265 \pm 0.0004$ pb	$(1.33 \pm 0.01) \times 10^5$ pb	$(8.3 \pm 0.07) \times 10^8$ pb
1000	$0.0264 \pm 0.02$ pb	$(0.8 \pm 0.6) \times 10^5$ pb	$(6.4 \pm 5) \times 10^8$ pb
10000	$0.0265 \pm 0.004$ pb	$(1.0 \pm 0.2) \times 10^5$ pb	$(7.9 \pm 0.9) \times 10^8$ pb
100000	$0.0265 \pm 0.002$ pb	$(1.3 \pm 0.05) \times 10^5$ pb	$(8.1 \pm 0.2) \times 10^8$ pb

TABLE B.8: proton collision producing two jets - Higgs vs Z and QCD-pole

The increase in statistic does indeed help us. In processes with more complicated pole structure however we would have to resort to unreasonably high event numbers. It is however not necessary to resort to too high statistics once we optimize on signal and background and combine the samples.

To conclude this appendix we have a look at Higgs production with associated tops at LHC. This is followed by subsequent decay of the Higgs to a  $b\bar{b}$  pair. The Likelihood analysis of this process can be found in [45]. We use it here simply as a test if our tool works correctly for something semi-realistic. The Feynman diagrams for the signal process and backgrounds (QCD and electroweak) are shown in B.1.

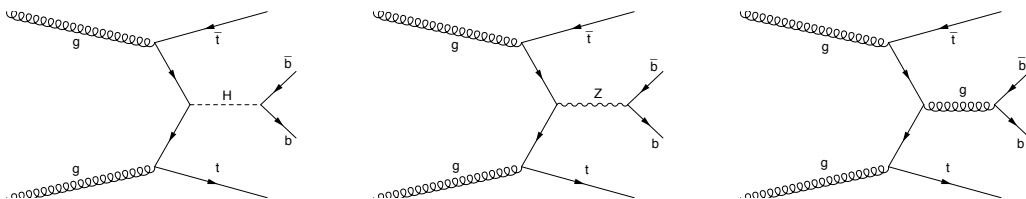


FIGURE B.1: Representative Feynman diagrams for the signal and the backgrounds. We have Higgs production with associated tops (left), the purely electroweak background (middle) and the QCD background (right).

We apply the standard cuts to the  $b\bar{b}$ -pair.  $P_T > 20\text{GeV}$ ,  $R_{bb} > 0.8$ ,  $\eta_b < 2.5$ ,  $110\text{GeV} < m_{bb} < 130\text{GeV}$ . Without the mass window we will not be able to even remotely map the phase space of the backgrounds right.

In the true simulation for the Log-Likelihood analysis its magnitude is mainly set by the detector resolution on the  $b\bar{b}$  pair. There we also apply a gaussian smearing to the propagator for the Higgs.

As it turns out we are evidently well equipped to produce a sample for the Higgs production with associated tops. Table B.9 summarizes our findings for different statistics.



No. events	signal	background 1	background 2
	$pp > htt, h > bb$	$pp > ttbb$ QED = 0	$pp > ttbb$ QCD = 0
MadGraph5	$0.329 \pm 0.0007$ pb	$0.432 \pm 0.001$ pb	$0.087 \pm 0.0003$ pb
1000	$0.338 \pm 0.05$ pb	$0.393 \pm 0.1$ pb	$0.09 \pm 0.06$ pb
10000	$0.328 \pm 0.004$ pb	$0.383 \pm 0.05$ pb	$0.075 \pm 0.008$ pb
100000	$0.328 \pm 0.0005$ pb	$0.383 \pm 0.03$ pb	$0.076 \pm 0.005$ pb

TABLE B.9:  $t\bar{t}$  Higgs production with decays to b's

This concludes our review of the accuracy of MadMax. Notice that we only considered processes with one or few subprocesses. This was done to save time and concentrate on the important features. For more subprocesses we only have to combine the single folders correspondingly. All this shows that MadMax apparently works properly - at least as a parallel integrator.

# Bibliography

- [1] K.Cranmer T.Plehn. Maximum significance at the lhc and higgs decays to muons. Eur. Phys. J. C51 415-420, arXiv 0605268 [hep-th], 2007.
- [2] The ATLAS Collaboration. Observation of a new particle in the search for the standard model higgs boson with the atlas detector at the lhc. Phys. Lett. B716 1-29, arXiv 1207.7214 [hep-ex], 2012.
- [3] The CMS Collaboration. Observation of a new boson at a mass of 125 gev with the cms experiment at the lhc. Phys. Lett. B 716 30, arXiv 1207.7235 [hep-ex], 2012.
- [4] A.Djouadi. The anatomy of electro-weak symmetry breaking i. Review, Phys.Rept 457 1-216, arXiv 0503172 [hep-ph], 2005.
- [5] J.Alwall M.Herquet F.Maltoni O.Mattelaer T.Stelzer. Madgraph 5 : Going beyond. arXiv 1106.0522 [hep-th], 2011.
- [6] J.Alwall P.Artoisenet S.de Visscher C.Duhr R.Frederix M.Herquet O.Mattelaer. New developments in madgraph/madevent. AIP Conf. Proc. 1078:84-89, arXiv 0809.2410 [hep-ph], 2008.
- [7] T.Plehn D.Rainwater. Higgs decay to muons in weak boson fusion. Phys. Lett. B520 108-114, arXiv 0107180 [hep-ph], 2007.
- [8] M.Srednicki. Quantum Field Theory. Cambridge University Press, 2011.
- [9] T.Plehn. Lectures on lhc physics. Lecture Notes, 2013.
- [10] J.Beringer et al. (Particle Data Group). Review of particle physics. Phys. Rev. D86, 010001, 2012.
- [11] P.Higgs. Broken symmetries, massless particles and gauge fields. Phys. Lett. 12, 132, 1964.
- [12] P.Higgs. Broken symmetries and the masses of gauge bosons. Phys. Rev. Lett. 13, 508, 1964.
- [13] M.Seymour. Quantum chromodynamics. Lecture Notes, arXiv 0505192 [hep-ph], 2005.
- [14] R.Ellis W.Stirling B.Webber. QCD and collider physics. Cambridge University Press, 2003.
- [15] M.Peskin D.Schroeder. An Introduction to Quantum Field Theory. Westview Press, 1995.
- [16] G.Altarelli G.Parisi. Asymptotic freedom in parton language. Nucl. Phys. B126 298, (1977).

- [17] A.Buckley J.Butterworth S.Gieseke D.Grellscheid S.Hoche H.Hoeth F.Krauss L.Lonnblad E.Nurse P.Richardson S.Schumann M.Seymour T.Sjöstrand P.Skands B.Webber. General-purpose event generators for lhc physics. Review Article, arXiv 1101.2599v1 [hep-ph], 2011.
- [18] J.Hammersley D.Handscomb. Monte Carlo Methods. Methuen's Monographs on Applied Probability and Statistics, 1975.
- [19] T.Sjöstrand S.Mrenna P.Skands. Pythia 6.4 - Physics and Manual. Lund University, Lund, 2006.
- [20] R.Kleiss R.Pittau. Weight optimization in multichannel monte carlo. Comput. Phys. Commun. 83 141-146, arXiv 9405257 [hep-ph], 1994.
- [21] C.Papadopoulos. Phegas: a phase-space generator for automatic cross-section computation. Comput. Phys. Commun. 137 247-254, arXiv 0007335 [hep-ph], 2000.
- [22] E.Byckling K.Kajantie. Reductions of the phase-space integral in terms of simpler processes. Phys. Rev. 187 Nr. 5, 1969.
- [23] F.Maltoni T.Stelzer. Madevent: Automatic event generation with madgraph. JHEP 0302 027, arXiv 0208156 [hep-ph], 2002.
- [24] I.Volobouev. Matrix element method in hep: Transfer functions, efficiencies and likelihood normalization. arXiv 1101.2259 [physics.data-an], 2011.
- [25] G.Bohm G.Zech. Introduction to statistics and data analysis for physicists. Lecture Notes, Verlag deutsches Elektronen-Synchrotron, 2011.
- [26] A.Read. Modified frequentist analysis of search results (the CL<sub>S</sub> method). CERN - Workshop on Confidence Limits, 2000.
- [27] The ATLAS Collaboration The CMS Collaboration The LHC Higgs Combination Group. Procedure for the lhc higgs boson search combination in summer 2011. Review, ATL-PHYS-PUB-2011-011, 2011.
- [28] K.Cranmer. Statistical challenges for searches for new physics at the lhc. arXiv 0511028 [physics.data-an], 2005.
- [29] K.Cranmer. LEPStats4LHC: Documentation and User Manual. Brookhaven National Laboratory - Department of Physics, Brookhaven, 2001.
- [30] J.Neyman K.Pearsons. On the problem of the most efficient tests of statistical hypothesis. Philosophical Transactions of the Royal Society of London. Series A, Containing Papers of a Mathematical or Physical Character. 231, 1932.
- [31] T.Junk. Confidence level computation for combining searches with small statistics. Nucl. Instrum. Meth. A434 435-443, arXiv 9902006 [hep-ex], 1999.
- [32] H.Hu J.Nielsen. Analytic confidence level calculations using the likelihood ratio and fourier transform. arXiv 9906010 [physics.data-an], 1999.
- [33] K.Cranmer B.Mellando W.Quayle Sau Lan Wu. Challenges in moving the lep higgs statistics to the lhc. arXiv 0312050 [physics.data-an], 2003.

- [34] M.Frigo S.Johnson. FFTW User's Manual 2.1.5. Massachusetts Institute of Technology, Cambridge, 2003.
- [35] H.Murayama I.Watanabe K.Hagiwara. Helas: Helicity amplitude subroutines for feynman diagram evaluations. Review, 2000.
- [36] T.Stelzer W.Long. Automatic generation of tree level helicity amplitudes. Comput. Phys. Commun. 81 357-371, arXiv 9401258 [hep-ph], 1994.
- [37] T.Plehn D.Rainwater D.Zeppenfeld. Determining the structure of higgs couplings at the lhc. Phys. Rev. Lett. 88:051801, arXiv 0105325 [hep-ph], 2001.
- [38] T.Figy S.Palmer G.Weiglein. Higgs production via weak boson fusion in the standard model and the mssm. JHEP 1202 105 , arXiv 1012.4789 [hep-ph], (2012).
- [39] T.Han B.McElrath.  $h \rightarrow \mu^+ \mu^-$  via gluon fusion at the lhc. Phys. Lett. B528 81-85, arXiv 0201023 [hep-ph], 2002.
- [40] T.Gleisberg S.Hoche F.Krauss M.Schonherr S.Schumann F.Siegert J.Winter. SHERPA manual. Hepforge, IPPP Durham, 2008.
- [41] A. Yildiz S.Glashow D.Nanopoulos. Associated production of higgs bosons and z particles. Phys. Rev. D18, 17241727, (1978).
- [42] J.Baglio A.Djouadi. Predictions for higgs production at the tevatron and the associated uncertainties. HEP 1010 064, arXiv 1003.4266 [hep-ph], (2010).
- [43] The D0 Collaboration. Combined search for the standard model higgs boson decaying to  $b\bar{b}$  using the d0 run ii data set. Phys. Rev. Lett. 109, 121802, (2012).
- [44] J.Butterworth A.Davison M.Rubin G.Salam. Jet substructure as a new higgs seach channel at the lhc. Phys. Rev. Lett. 100 242001, arXiv 0802.2470 [hep-ph], 2008.
- [45] T.Plehn P.Schichtel D.Wiegand. Madmax, or where significance can come from. in preparation, 2013.
- [46] LHC Higgs Cross Section Working Group. Handbook of lhc higgs cross sections: 1. inclusive observables. Report, arXiv 1101.0593 [hep-ph], 2011.
- [47] R. Cousins V.Highland. Incorporating systematic uncertainties into an upper limit. Nucl. Instrum. Meth. A320 331335, 1992.
- [48] K.Cranmer. Frequentist hypothesis testing with background uncertainty. arXiv 0310108 [physics.data-an], 2003.
- [49] A.Djouadi J.Kalinowski M.Spira. Hdecay: a program for higgs boson decays in the standard model and its supersymmetric extensions. Comput. Phys. Commun. 108 56-74, arXiv 9704448 [hep-ph], 1997.
- [50] The ROOT Team. ROOT Users Guide 5.21. CERN, Geneva, 2008.



# Erklärung

Ich versichere, dass ich diese Arbeit selbstständig verfasst und keine anderen als die angegebenen Quellen und Hilfsmittel benutzt habe.

Daniel Wiegand

Heidelberg, den 20. Oktober 2013